ACS OMEGA

Open Access

http://pubs.acs.org/journal/acsodf

Article

Valorization of Lubrication Oil and Cooking Oil via Catalytic Copyrolysis with Ni Doped on Activated Carbon

Witchakorn Charusiri,* Naphat Phowan, and Tharapong Vitidsant

Cite This: *ACS Omega* 2025, 10, 14699−14722

Read Online

ACCESS | Metrics & More | Article Recommendations

ABSTRACT: The aim of the copyrolysis of used lubricant oil (ULO) and used cooking oil (UCO) was to investigate the effects of operating parameters on the thermal stability of ULO and UCO, which significantly improves the quality of fuel-like products. This process was carried out in a 3000 cm^3 semibatch pyrolysis reactor; the systematic experimental design involved catalytic copyrolysis by varying the operating parameters of the pyrolysis temperature (400−500 °C), the inert nitrogen flow rate (25−150 mL/min), and the ratio of blended ULO/UCO from 0.9:0.1 to 0.2:0.8. The advantage of Ni modified to activated carbon is that it is considered a stronger acid solid catalyst with an extraordinary pore structure, which undergoes catalytic copyrolysis; the concentration of the Ni metal doped into the AC catalyst was 3−10 wt %, and the catalyst loading on the feedstocks (5−20 wt % of Ni/AC catalyst) was performed. The effects of the conversion of ULO/UCO on the yield and physicochemical properties of copyrolysis oil and the product distribution according to ASTM D86 were investigated. The 5 wt % Ni doped into the AC catalyst is related to the strength of the acid activity that accelerated the conversion of large hydrocarbon compounds to obtain a straight aliphatic hydrocarbon compound, and the Ni/AC catalyst also plays a role in facilitated C−C bond cleavage and bond scission to smaller hydrocarbon compounds. The highest yield of naphtha-like fraction of 25.34 wt % was obtained at the optimal condition of 425 °C, the N_2 carrier flow rate was 50 mL/min, the ULO/UCO ratio was 0.5:0.5, 5 wt % Ni was modified into the AC catalyst, and 5% catalyst was loaded into the feedstock. The synergistic effects of UCO and ULO during copyrolysis also revealed that the H-donor and hydrocarbon radicals of UCO decrease the thermal stability of ULO, whereas the addition of 5 wt % Ni to the AC catalyst, which is relevant to acid activity, is mainly responsible for bond scission, hydrogenation, isomerization, and oligomerization, resulting in the formulation of condensable volatile vapors to maximize the production of straight aliphatic and olefinic hydrocarbon compounds, which can be used as sustainable fuels from the conversion of waste to alternative energy.

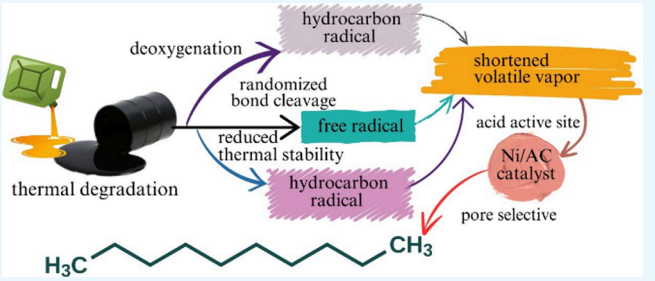

1. INTRODUCTION

The rapid growth of the world economy over the past decade has led to the expansion of urban communities and societies, while the development of the world economy has resulted in an increasing trend in the production of products for daily life consumption and has inevitably caused more waste and environmental impact.[1] Used cooking oil (UCO), which includes oils discarded after food processing, cooking, or frying in restaurants and households, has been increasing rapidly each year. There are no clear reports or doubts about the collection, treatment, and disposal of these waste cooking oil.[2] UCO should be properly collected and disposed of after multiple uses due to thermal oxidation, impurities, and contamination. In fact, improperly reusing UCO poses health risks.[3] Furthermore, treating and disposing of UCO often leads to illegal dumping, which has severe environmental impacts.[2,3]

The valorization of UCO is desirable for upgrading waste oil to its value chemicals or circulation to serve as alternative fuels. Numerous studies have conducted experiments on the utilization of leftover cooking oil, which typically has well-known positive impacts on the environment, such as the conversion of waste to high-value fuels and chemicals.[4,5]

In recent years, the production of methyl esters from UCO has been encouraged for blending with diesel to promote sustainable fuel production. However, trans-esterified biodiesel has several disadvantages, such as a low calorific value due to the high moisture content in raw UCO and difficulty in removing oxygen from fatty acids.[5,6] Additionally, byproducts, such as crude glycerol, wastewater, and chemicals, can have adverse environmental effects if accidentally released.

Received: September 3, 2024
Revised: February 28, 2025
Accepted: March 18, 2025
Published: April 9, 2025

Deoxygenation of UCO improves thermal stability of biofuel but requires additional conditions such as supercritical reactions, hydrothermal liquefaction processes, or catalytic cracking reaction.[5−7] Owing to its low H/C ratio and a high O/C ratio, UCO has high viscosity and poor thermal stability.[6,7] Catalytic pyrolysis is therefore a promising technology for improving the conversion of UCO into hydrocarbon-rich oils (C_3 to C_{24})[7,8] and improving fuel quality by reducing the oxygen content through rapid cracking and catalytic reforming.

Used lubricant oil (ULO) is classified as a waste containing polyaromatic hydrocarbon compounds and impurities.[9] Despite the increasing waste, only 25−40% of ULO is properly collected and treated worldwide.[10] Thailand's law stipulates ULO as hazardous waste that must be properly disposed of to prevent environmental impacts.[3,10]

One promising method for managing ULO is converting it into energy and valuable chemicals via pyrolysis, a thermochemical reaction that breaks down large hydrocarbon chains in the absence of oxygen.[9,10] The use of catalysts, e.g., zeolite, sulfated zirconia, and FCC catalysts, accelerate thermal decomposition and catalytic cracking producing appropriate condensable volatile vapors,[11] which may further react with the catalyst under appropriate conditions to obtain a fuel-like oil consisting of C_5−C_{11} (naphtha-like), C_{11}−C_{15} (kerosene-like), and C_{15}−C_{19} (diesel-like).[11,12] Meanwhile, the yield of C_{19}+ hydrocarbon is affected by depolymerization and causes aggregation into large hydrocarbon compounds.[12]

The rapid growth of waste oil from frying and lubricants is poorly managed, causing an environmental impact such that the world is facing challenges in converting this waste into sustainable energy. Copyrolysis has attracted much attention for its advantages in terms of raw feedstock availability, which involves two or more raw feedstocks. The initial thermal degradation of a large hydrocarbon compound produces free radicals, which enhances the decomposing of large hydrocarbons via the bond scission into high quality for fuel-like pyrolysis oil,[13,14] effectively enhancing the synergy in pyrolyzed oil and establishing valuable chemicals.

Understanding copyrolysis is important for reducing cost and environmental impact; waste residues with high H/C ratios are introduced into the pyrolysis of individual hydrocarbons with lower H/C ratios via feedstocks with higher H/C ratios.[15] Catalytic copyrolysis enhances the catalytic activity to produce high-quality straight alkane compounds.[16,17] However, there is limited information about the copyrolysis of waste oil, which is possible in commercial establishments. Therefore, it is essential to investigate the catalytic activity, an agile preparation, low cost, catalytic performance, and reusable catalysts for the pyrolysis of both waste oils to produce the desirable fuel-like properties.[17]

A previous study on the copyrolysis of a lubricant and plastic waste[18] illustrated that their interactions affect product distribution in the diesel-like fraction. The thermal decomposition of large hydrocarbon chains facilitates degradation and provides an H-donor for free radical reactions, while the use of lubricant oil for copyrolysis enhances the capabilities of mass and heat transfer,[11,19] accelerates both the degradation of their radicals and the formation of long-chain hydrocarbons into the moderate hydrocarbon chains, and reacts with the active site of the catalyst resulting in enhanced quality of the pyrolysis oil that could be enhanced by incorporating catalysts such as zeolite, which is promising as a reactive catalyst that is used in copyrolysis reactions for large hydrocarbons.[20−24] Nevertheless, zeolite has some limitations due to the tendency for coke deposition on its surface, resulting in deactivation of the catalyst.[20]

Active carbon (AC) has a large specific surface area and wide pore size distribution due to its amorphous carbon structure, which consists of covalent bonds and aromatic conformations resembling tightly packed carbon sheets depending on the material, preparation, and activation techniques.[25−27] AC has the advantages of being a wide source, being low cost, and having an easily modified and stable chemical structure[28,29] that is capable of being loaded with metal oxides.[29−31] Metal doping of AC enhances the catalytic activation of C−C and C−H bonds, increases acid active sites,[26,28] and improves the catalytic activity.[29,32] There is a study of NiO catalysts for removing oxygen from oxygen-containing compounds.[32,33] The propensity for impregnated NiO active sites into AC-favorable catalytic copyrolysis is related to the strength of the acid activity that accelerates the conversion of large hydrocarbon compounds, enhancing deoxidation to produce hydrocarbon-rich pyrolyzed oils and also obtain aliphatic and olefinic hydrocarbon compounds,[33−35] such as naphtha-like compounds from C_5−C_9 hydrocarbons and C_9−C_{15}, which exhibit kerosene-like properties, whereas pyrolyzed oils composed of C_{15}−C_{18} hydrocarbon compounds are classified in a diesel-like range.[27,30,32,33,36]

This research therefore changes the perspective of the copyrolysis of ULO with UCO blended by using an active heterogeneous catalyst, which is an acid catalyst, and the preparation of an active metal doped into activated carbon for use in the copyrolysis of ULO with UCO blended, which is essential for investigating the low-cost material[2] that illustrated a catalytic effect to enhance the decarbonylation, decarboxylation, and secondary cracking reaction, also promotes the formation of aliphatic and olefin hydrocarbon compounds,[17,26−28] while the acidity and pore structure of the catalysts are enhanced to catalyze the degradation of C−H and C−C bonds in both ULO and UCO.[9,17,25] Thus, the Ni doped into the AC catalyst enhances the deoxidation ability of ULO/UCO to produce hydrocarbon-rich pyrolysis oil.[30,32,34,35] Furthermore, the synergistic effects during copyrolysis are employed to comprehensively understand the copyrolysis process to improve the value of waste management from the perspective of energy sustainability and a circular economy according to the guidelines for developing the economy and high-value industries or the S-curve trend of Thailand's economic development.

2. MATERIALS AND METHODS

2.1. Raw Materials. The waste lubricants and UCO were collected during February−April 2023 and were obtained from an automobile service center (Bangkok, Thailand) and from the university canteen (Bangkok, Thailand), respectively. First, both types of collected oil sample were sieved by using a 25-mesh screen to remove residual material during its utilization and operation. The moisture content of the oil samples was measured upon heating the samples via an air oven at the operating temperature of 105 °C for 24 h according to the American Oil Chemists' Society (AOCS) official method Ca 2c-45.[36,37] This method involves determining the moisture and volatile matter contents of commercial fats and oils. After that, the samples were then stored in opaque plastic bottle bottles and purged with nitrogen gas to ensure the absence of oxygen

https://doi.org/10.1021/acsomega.4c08111
ACS Omega 2025, 10, 14699−14722

to prevent chemical oxidation and stored at standard room temperature without further purification.

The elemental analysis of the used oil was performed via a LECO CHNS-628 analyzer (LECO Corp., USA) to determine the amounts of carbon, hydrogen, nitrogen, and sulfur, whereas the oxygen content in a sample was determined via the difference calculations. The physicochemical analyses of both ULO and UCO using a DV-3 Ultra Brookfield digital viscometer (Brookfield, Japan) at 40 °C determined the kinematic viscosity in accordance with ASTM D445. Titrino plus 848 automated titration (Metrohm AG, Germany) was performed via automated potentiometric titration using a 0.001 M KOH standard solution and 50 mL of acetone to titrate 10 g of sample to determine the acidity value of the oil sample in accordance with ASTM D664. The calorific values were determined with a LECO AC500 bomb calorimeter (LECO Corp., USA) in accordance with ASTM D240 and comparison with the calorific value obtained from the calculated via Dulong's equation:[14]

$$\mathrm{HHV\ (MJ/kg)} = 0.338\mathrm{C} + 1.428\left(\mathrm{H} - \frac{\mathrm{O}}{8}\right) + 0.095\mathrm{S} \quad (1)$$

GC-MS analyses of both raw ULO and UCO were carried out via an Agilent GC7890/GCMS5978 gas chromatograph with a mass spectrometer (Agilent Technologies, Inc., USA). The samples of ULO and UCO were subsequently diluted with CS_2 (Sigma-Aldrich, Singapore) at a ratio of 1:100, after which 1 μL of sample was injected into the GC7890 instrument equipped with both an FID and a thermal conductivity detector and a split/splitless injection unit. An HP-5 capillary (30 m × 0.25 mm × 100% dimethylpolysiloxane film thickness of 0.25 μm) polar column (JW Scientific, USA) coupled with a 5977A mass spectrometer (electron ionization at 70 eV, mass range of 33−500 m/z) was employed. The temperature of the oven was set to 320 °C. The NIST mass spectral libraries (National Institute of Standards and Technology, USA) were used to determine the characteristic chromatographic peaks.

2.2. Catalyst Preparation and Characterization. AC was obtained from the Centre of Fuels Research and Energy from Biomass (Chulalongkorn University, Thailand). The preparation of biochar-activated carbon was prepared by carbonization of waste empty palm kernels at 350−400 °C for 3 h and then physical activation via heat steam at a temperature of 900 °C for 3 h. Chemical activation was performed via the addition of KOH at a ratio of KOH to biochar (1:3) at an activation temperature of 850 °C for 3 h.[38]

In this study, AC was used as a catalyst with a size of 20−40 mesh. The AC was modified with $Ni(NO_3)_2{\cdot}9H_2O$ (Sigma-Aldrich, Singapore). x%Ni-AC was measured, where x is the percentage of doped metal oxide embedded into the AC template via wet impregnation. A total of 10 g of AC was weighed, and deionized (D.I.) water was added to the AC until it was saturated, after which it was filtered through a vacuum filter for 3 h. The predominant weight of $Ni(NO_3)_2{\cdot}9H_2O$ was dissolved according to the percentage of metal oxide to be impregnated over the AC with 15 mL of DI water until completely dissolved. Then, a $Ni(NO_3)_2$ solution was slowly added, and the mixture was stirred thoroughly onto the AC, which was repeated four times. After that, the samples were rinsed with 10 mL of D.I. water two times, washed with 10 mL of D.I. water to the impregnated activated carbon, left for 10 min, and filtered with a vacuum filter. The obtained x%Ni-AC was treated by drying in an oven at 80 °C for 3 h and drying overnight at 120 °C. Prior to the experiment, the Ni/AC was activated in a muffle furnace and calcined at 500 °C at a heating rate of 10 °C/min under an inert N_2 carrier gas for 90 min. X-ray diffraction patterns were used to investigate the crystal structure of the samples, which were obtained with a D8 Advance diffractometer (Bruker, USA) with a Cu Kα radiation source (λ = 0.15406 nm) operating at 40 kV and 40 mA. The scattering angle ranged $5° \leq 2\theta \leq 60°$, and the scanning rate was 4°/min. An EDX-720 energy-dispersive X-ray spectrometer (Shimadzu, Japan) and an S8 TIGER X-ray fluorescence spectrometer (Bruker Corp., Germany) were used to determine the elemental analysis and chemical characterization that can be applied to select any part of the catalyst surface. The morphological characteristics of the catalysts were measured via Brunauer−Emmett−Teller (BET) nitrogen adsorption−desorption analysis at 77 K by an ASAP 2020 instrument (Micromeritics Instrument Corp., USA). Prior to BET analysis, the catalyst samples were dried overnight at 105 °C and degassed at 573.15 °C for 6 h to remove any moisture residue or impurities. The total surface area pore volume, pore volume, and average pore size were calculated.

2.3. Experimental Procedures. The cofeedstocks of ULO and UCO were converted by thermal decomposition, catalytic cracking, and subsequent secondary reactions to obtain the desired light hydrocarbon composition at C_5−C_{11}. This reaction was performed via an absence of oxygen atmosphere and H_2 free deoxygenation using an inert N_2 carrier gas. The apparatus for the catalytic copyrolysis reaction is depicted in Figure 1.

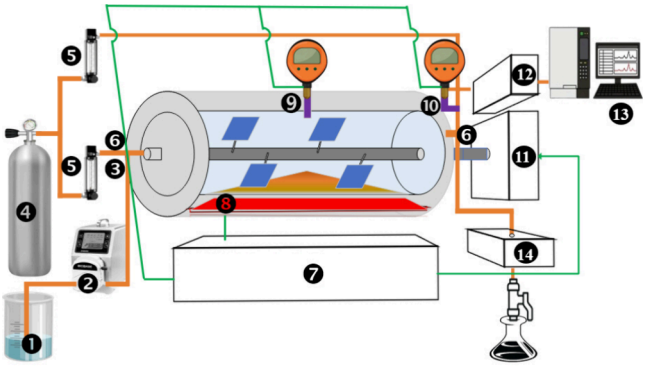

Figure 1. Schematic diagram of the copyrolysis of ULO/UCO in a semibatch pyrolyzer.

The pyrolysis experiments were carried out in a custom-built electrically heated stainless-steel semibatch reactor with a volume of 3000 cm^3, a K-type thermocouple located at the middle of the pyrolyzer, and the gas outlet involved to monitor the temperature during the reaction and the volatile vapor temperature.

A semibatch reactor equipped with a cooling unit was used to separate the condensed hydrocarbon form of the entrained pyrolysis oil and uncondensed volatile gases. While the

https://doi.org/10.1021/acsomega.4c08111
ACS Omega 2025, 10, 14699−14722

noncondensable gases passed through the gas drying unit, the noncondensable gases were also collected to analyze the composition via GC-FID. Prior to the catalytic reaction, the Ni/AC catalyst was added to the reactor at 1−20 wt % by placing it on top of a quartz wool inside the reactor, which was used to separate solid residue that was not completely pyrolyzed. Then, nitrogen gas was introduced through the Ni/AC packed bed to the pyrolyzer for several times as a carrier to ensure that the reaction occurred in an oxygen-free atmosphere in the pyrolyzer to avoid oxidative degradation and minimize devolatilization reactions.[27,28,32,35] The pyrolyzer was then allowed to supply inert nitrogen gas as a carrier at a flow rate of 20−200 mL/min. The reaction temperature was controlled via a PID controller and was preheated from room temperature to the predetermined temperature at a rate of 10 °C min^{-1}.

The designated ratio of the cofeedstock was subsequently pumped into the reactor at a constant rate of 10 mL/min via a peristaltic pump. The reactor was agitated under constant stirring for a predetermined reaction time until the reaction was finished. The volatile vapor that cracked during the copyrolysis reaction passed through the catalyst and flowed out of the inert nitrogen gas to the gas outlet and therefore condensed in the system of condensers, which provided a lower temperature that was created by the circulation of ice water inside the condenser tube, which was used to separate the condensable volatile gaseous form of the entrained pyrolysis oil and the uncondensed volatile gases. The condensable liquid oil was eventually transferred to a flask at the end of the unit for further analysis.

2.4. Product Yield and Composition Analysis. The mass balance of the copyrolysis reaction was established by weighing the liquid condensate (M_2), and the solid residues containing both the spent catalyst (M_3) and the pyrolysis residue (M_4) at the end of the reaction were collected and weighed when the temperature of the pyrolyzer was cooled to room temperature. The yield of liquid pyrolysis oil was calculated by weighing the difference between the collector before (M_1) and after copyrolysis (M_2). The remaining coke yield was collected from the pyrolyzer and weighed according to the change in mass before and after catalyst copyrolysis. The weight of the noncondensable gas was calculated via the difference calculation as a mass balance.

The yield of each designated product (liquid, solid, or gas) was defined via eqs 2 to 4 and calculated via the corresponding mass divided by the initial reactant mass.

$$\%Y_{liquid} = \frac{M_2}{M_1} \times 100\% \quad (2)$$

$$\%Y_{solid} = \frac{M_4 - M_3}{M_3} \times 100\% \quad (3)$$

$$\%Y_{gas} = 100\% - (Y_{liquid} + Y_{solid}) \quad (4)$$

where M_1, M_2, M_3, and M_4 represent the mass change of the initial oil, the mass of the pyrolyzed oil, the mass of the catalyst, and the total solid mass obtained from the reactor, respectively.

Analysis of the condensable pyrolyzed oil was used to determine the chemical composition and predict the optimal conditions from its composition. GC/MS analyses were performed via an Agilent GC7890/GCMS5978 gas chromatograph with a mass spectrometer (Agilent Technologies, Inc.) equipped with an HP-5 MS capillary column (30 m length × 0.25 mm i.d. × 0.25 μm thickness of 5% diphenyl and 95% dimethylpolysiloxane). The compounds were identified on the basis of peak matching of the mass spectra from the NIST library.

The pyrolysis oil was characterized via simulated distillation gas chromatography (DGC) according to ASTM D86, which represents the composition of pyrolysis oil according to its boiling point range of crude oil; an Agilent GC7890A gas chromatograph (Agilent Technologies, USA) coupled with a DB-1 capillary (10 m length × 0.53 mm i.d. × 2.65 μm thickness of 100% dimethylpolysiloxane) nonpolar column (J&W Scientific, USA) was used for determination. The analyses of pyrolysis oil determined according to the crude oil boiling temperature range[18,36] illustrated the distillate fraction from C_5 to C_{11} that was obtained from the initial boiling point to 200 °C, which is known as the naphtha-like or gasoline-like fraction.

C_{11}−C_{15} presented kerosene-like properties at the boiling point range from 200 to 250 °C, while the light gas oil fraction was identified at the boiling point of 250 to 300 °C, and the gas oil fraction was identified at the boiling point between 300 and 370 °C.[18,36] In general, the boiling temperature range from 250 to 370 °C is also used to classify the diesel-like properties of carbon ranging from C_{15} to C_{19} hydrocarbon compounds[30,33] while the simulated distillation fraction obtained from the boiling temperature over 370 °C is defined as a long residue (>C_{19}).[38] Additionally, elemental analysis of the liquid products was performed via a LECO CHNS-628 analyzer (LECO Corp. USA) to determine the amounts of carbon, hydrogen, and nitrogen. The oxygen levels in the samples were obtained via calculations different from those of the ultimate analysis. Furthermore, the physicochemical analyses and fuel properties of the pyrolyzed CPO were determined. The kinematic viscosity was analyzed in accordance with ASTM D445 using a DV-3 Ultra Brookfield digital viscometer (Brookfield, Japan) at 40 °C, and the caloric values were determined via a LECO AC500 bomb calorimeter in accordance with ASTM D240.

2.5. Synergy of the Copyrolysis Study. To further understand the copyrolysis, which possibly enhances the pyrolysis oil yield and fuel properties, the synergy of blended ULO with UCO during the copyrolysis reaction was investigated by comparing the actual yield from the experiment with the theoretical yield value via the additivity rule from the proportional yield average results according to the individual components.[28,39] Generally, the feedstock blend ratio is the most important parameter affecting the synergistic effect, which can be used to determine the influence of the interaction of the ULO blending ratio with UCO, which results in a greater or lesser effect than that obtained by the actual product yield of both specific cofeedstocks and individual feedstocks. Therefore, each product distribution of yield percentage (Y_{exp}) was obtained experimentally through copyrolysis of ULO and UCO, and the theoretical values (Y_{theo}) were calculated via eq 5:

$$Y_{theo} = Y_1M_1 + Y_2M_2 \quad (5)$$

where Y_1 and Y_2 represent the actual product distribution on the %yield obtained from the catalytic pyrolysis of individual components, and M_1 and M_2 are the mass molar ratios of the ULO and UCO, respectively, in the copyrolysis of the blends,

https://doi.org/10.1021/acsomega.4c08111
ACS Omega 2025, 10, 14699−14722

whereas Y_{Exp} is the experimental value from the copyrolysis of the blends. The deviation value (ΔY) of the yield of each product distribution between the experimental and theoretical results was used to calculate the synergistic efficiency during copyrolysis, as shown in eq 6:

$$\Delta Y = Y_{exp} - Y_{theo} \quad (6)$$

The value of ΔY represents the strength of the synergistic reaction. As shown in eq 6, if the experimental value is greater than the theoretical value, then the blended cofeedstocks enhance the positive effect on the copyrolysis product yield. When the deviation value is equal to zero, there is no interaction of the blended cofeedstocks when the deviation value <0; a negative synergy or inhibitory effect can be used to determine the possible chemical pathway.

3. RESULTS AND DISCUSSION

3.1. Characterization of Feedstock. The proximate analyses of ULO and UCO were carried out according to the ASTM D121 standard, while the AOCS official method Ca 2c-45 involves determining the moisture and volatile matter contents of commercial fats and oils via an air oven. The volatile matter contents of ULO and UCO were high at 96.32 and 96.81 wt %, respectively. The ash content was relatively low: 2.31 and 1.13 wt % for the ULO and UCO samples, respectively. the moisture contents of ULO and UCO were 1.37 and 2.06 wt %, respectively.

The ultimate analysis of the ULO revealed a relative content of carbon of 82.07 wt %, hydrogen of 15.11 wt %, and oxygen of 2.82 wt %. A relatively negligible amount of oxygen could be formed by oxidation in air during operation. The UCO contains 71.77 wt % carbon, 10.82 wt % hydrogen, and 16.38 wt % oxygen. Notably, UCO contains only a small amount of nitrogen (1.03 wt %), which may be caused by oxidation from fried protein-rich food.[2,4]

Both the UCO and ULO do not contain any sulfur, but the ULO may actually be contaminated with sulfur from the combustion vapors of the diesel fuels. Therefore, the negligible sulfur content is less than the limit of detection. The H/C and O/C mass molar ratios and the higher heating values of both the ULO and UCO were calculated and are presented in Table 1.

Additionally, the HHV analysis according to the adiabatic bomb calorimeter indicates that both the ULO and UCO have higher calorific heating values of 42.5 and 36.01 MJ/kg, respectively. Moreover, the ULO presented an HHV (42.5 MJ/kg) and H/C mass/molar mass ratio (2.21), which resulted in a higher value than did the UCO (36.01 MJ/kg and H/C mass/molar ratio of only 1.81), which is beneficial to the pyrolysis process;[10,11,15] when the ULO is involved in the copyrolysis, the higher heating value and H/C mass/molar ratio of the ULO are introduced into the other feedstock, which results in a lower HHV and H/C ratio to improve the process of catalytic pyrolysis to increase the production of copyrolyzed oil and its fuel-like properties.[16,18,39,40]

Table 2 shows that the ULO and UCO, which are used as raw feedstocks for catalytic copyrolysis, present a peak intensity greater than 0.5% at a retention time of 10−40 min. The total % peak intensity consists of carbon ranging from C_{12} to C_{35} at 68.47%, whereas the UCO mainly comprises carbon ranging from C_{10} to C_{18} at a retention time ranging from 8 to 17 min, which represents a total % peak intensity of 61.81% and consists of oleic acid and palmitic acid, similar to the previous characterization of UCO via GC/MS techniques.[36]

Table 1. Ultimate Analyses of UCO and ULO

components	raw ULO	raw UCO	standard method
proximate analysis (wt %)			
moisture	1.37	2.06	AOCS Ca 2a-45
volatile	96.32	96.81	ASTM D121
ash	2.31	1.13	ASTM D121
ultimate analysis (wt %)			ASTM D987
C	82.07	71.77	
H	15.11	10.82	
O	2.82	16.38	
N	n.d.	1.03	
S	n.d.	n.d.	
H/C	2.21	1.81	calculation
O/C	0.03	0.17	calculation
HHV[a]	48.81	36.79	calculation
HHV	42.50	36.01	ASTM D240
kinematic viscosity	106.49	58.89	ASTM D445-19

[a]Calculated using HHV (MJ/kg) = 0.338C + 1.428[H − (O/8)] + 0.095S.

Table 3 presents the product distributions of the cofeedstocks obtained via simulated DGC according to the boiling temperature range. The results revealed that both the ULO and UCO contained mainly gas oil-like fractions and long residues with complex structures and large hydrocarbon molecules.[18,26,41] Additionally, the results were consistent with those of the GC/MS analysis, whereas both ULO and UCO before the copyrolysis process contained carbon molecules from C_{16} to C_{40}. Thus, the analyses of raw feedstocks of both the ULO and UCO revealed high viscosity properties that cannot be directly used as fuels in an internal combustion engine.[18,42,43]

3.2. Catalyst Characterization. In general, activated carbon can be produced by physical or chemical activation processes during the carbonization of palm oil kernels, and the resulting activation reaction can lead to the transformation of the Sp^2 or Sp^3 carbon hybridization structure with other elements that are also formed on the surface of activated carbons,[25] resulting in increased acid activity in the catalytic reactions. In this study, AC was employed in the production of both smaller paraffin and olefin hydrocarbons from the catalytic cracking of large hydrocarbon molecules and was recognized for its excellent deoxygenation properties and mesopore structure. Acidic sites enhance the catalysis of C−C and C−O bond degradation in UCOs, affecting the production of hydrocarbon components.[17,25] The introduction of NiO active sites to establish NiO-doped AC catalysts enhanced the stronger acidity and more developed pore structure of Ni/AC, demonstrating its ability in the deoxygenation reaction, and further catalytic pyrolysis enhances C−O bond cleavage rather than C−C cleavage,[43,44] which then passes through the mesoporous AC and undergoes a secondary reaction.[45] Figure 2 shows the XRD patterns of the activated carbon catalyst and the 5 and 10 wt % of Ni impregnated on activated carbon compared with the XRD patterns of the carbon catalysts.

The XRD pattern of AC and Ni doped into the support AC showed a broad diffraction peak at 2θ values ranging from 18 to 29°, indicating that the degree of graphitization of AC was relatively low and represented a mostly amorphous structure.[45]

https://doi.org/10.1021/acsomega.4c08111
ACS Omega 2025, 10, 14699−14722

Table 2. GC/MS Analyses of the Raw Material

RT (min)	peak intensity (%) ULO	peak intensity (%) UCO	chemical compounds	chemical formula
8.072	0.93		hexadecane	$C_{16}H_{34}$
8.536			1.2-dibutylcyclopentane	$C_{13}H_{26}$
8.611			3-heptadecene	$C_{17}H_{34}$
8.649			heptadecane	$C_{17}H_{36}$
8.890	6.21		diethyl phthalate	$C_{12}H_{14}O_4$
8.927			heptadecane	$C_{17}H_{36}$
9.569			1-nonadecene	$C_{19}H_{38}$
9.703			2-heptadecanone	$C_{17}H_{34}O$
9.725	0.94		2-propenoic acid, 2-methyl-, decyl ester	$C_{14}H_{26}O_2$
9.736			2-heptadecanone	$C_{17}H_{34}O$
10.103		6.73	*n*-hexadecenoic acid	$C_{16}H_{32}O_2$
10.158	0.57		eicosane	$C_{20}H_{42}$
10.377	1.23		hexadecanoic acid, methyl ester	$C_{17}H_{34}O_2$
10.613			heneicosane	$C_{21}H_{44}$
10.872		4.44	*n*-octadecenoic acid	$C_{18}H_{36}O_2$
11.320			eicosane	$C_{20}H_{42}$
11.397	1.5		1-iododotriacontane	$C_{32}H_{65}I$
11.410	2.27		(*E*)-9-octadecenoic acid, methyl ester	$C_{19}H_{36}O_2$
11.558		3.29	palmitoyl	$C_{16}H_{31}OCl$
11.785	1.39		tetracontane	$C_{40}H_{82}$
11.830	2.32		(*E*,*E*,*Z*)-1,3,12-nonadecatriene-5,14-diol	$C_{19}H_{34}O_2$
11.950	2.82		9-methylnonadecane	$C_{20}H_{42}$
12.235	3.45		tetratetracontane	$C_{44}H_{90}$
12.308		4.73	9-octadecenal	$C_{18}H_{34}O$
12.477	1.26		tetracosane	$C_{24}H_{48}$
12.485			2,4-dimethyleicosane	$C_{22}H_{46}$
12.854	0.63		tricosane	$C_{23}H_{48}$
12.903			1-tetracosene	$C_{24}H_{50}$
12.947			1-hexacosene	$C_{18}H_{38}$
12.982			2-methylhexacosane	$C_{26}H_{52}$
12.990			3-methylheptadecane	$C_{27}H_{56}$
13.218			docosane	$C_{22}H_{46}$
13.490	4.08		tritetracontane	$C_{43}H_{88}$
13.630	5		octacosane	$C_{28}H_{57}$
14.005	2.23		octacosane	$C_{28}H_{58}$
14.061			2-methyloctadecane	$C_{19}H_{40}$
14.115	5.05		3-methyloctadecane	$C_{19}H_{40}$
14.380	5.28		pentatriacontane	$C_{35}H_{72}$
16.225	4.04		fumaric acid, 2-methylallyl pentadecyl ester	$C_{23}H_{40}O_4$
16.285	4.48		undec-10-ynoic acid, octadecyl ester	$C_{29}H_{54}O_2$
16.870	4.23		sulfurous acid, octadecyl 2-propyl ester	$C_{21}H_{44}O_3S$
16.960	4.52		2-methyltetracosane	$C_{25}H_{52}$
17.055	4.04		2-methyltetracosane	$C_{25}H_{53}$
18.779		2.11	tridecane	$C_{13}H_{16}$
20.558		0.86	*n*-decanoic acid	$C_{10}H_{20}O_2$
21.215		0.59	7-tetradecene	$C_{14}H_{28}$
21.423		1.73	tetradecane	$C_{14}H_{30}$
22.654		0.94	1-butyl-2-pentylcyclopentane	$C_{14}H_{28}$
23.927		18.03	pentadecane	$C_{15}H_{32}$
25.159		0.84	*n*-nonylcyclohexane	$C_{15}H_{30}$
26.277		1.09	hexadecane	$C_{16}H_{34}$
28.165		0.75	8-heptadecene	$C_{17}H_{34}$
28.520		3.92	heptadecane	$C_{17}H_{36}$
32.728		1.24	2-heptadecanone	$C_{17}H_{34}O$
33.918		9.97	*n*-hexadecanoic acid	$C_{17}H_{34}O_2$
40.959		0.55	(*Z*)-9-octadecenamide	$C_{18}H_{35}NO$

Table 3. Analyses of the ULO and UCO According to ASTM D86

boiling point range (°C)	product fraction	wt % of fraction ULO	wt % of fraction UCO
initial temperature−200 °C	naphtha (C_5−C_{11})	0.00	0.00
200−250 °C	kerosene (C_{11}−C_{15})	0.15	0.00
250−300 °C	light gas oil (C_{15}−C_{19})	1.85	4.45
300−370 °C	heavy gas oil (C_{19}+)	7.00	10.65
370 °C−final temperature	long residue (C_{33}+)	91.00	85.00

The presence of NiO in the cubic crystalline structure, with diffraction peaks at 2θ values of 38.90 and 43.28°, which are associated with the presence of amorphous or graphitic carbon, results in pore blockage in the support (JCPDS No. 01-075-2078),[46,47] and the 2θ value at 43.28° illustrates the presence of nickel oxide (JCPDS No. 01-078-0429), confirming that the support structure of the parent activated carbon has been modified with nickel metal successfully.[47] Additionally, the diffraction peak at 2θ represents the same pattern as that of the parent activated carbon, which illustrates that the deposition of nickel to the parent template of AC does not significantly change the support structure;[48] therefore, the XRD pattern of Ni impregnated with AC illustrates NiO peaks because the metallic nickel phase is also detected with diffraction peaks at 2θ values of 38.90 and 43.28°, and the peak intensity is lower than the XRD pattern of activated carbon, which could be due to very low metal loading and the even distribution of NiO into the porous structure or because the crystal size is smaller and results in high dispersion of NiO in the catalyst, resulting in the facile occurrence of mesopore blockage.[3,45,46]

Furthermore, notably, the increase in the concentration of Ni doped from 5 to 10 wt % has no effect on the change in intensity or peak position, which does not affect the chemical structure of the activated carbon. The crystallite sizes of NiO slightly varied with varying NiO contents in the samples. For the modification of Ni to AC catalysts, 5% NiO/AC and 10% NiO/AC had the smallest crystallite sizes of NiO and resulted in the highest specific surface area among the metal oxide catalysts. For other mixed oxide catalysts, there is a relationship between the catalyst crystallite size and the specific surface area. These results correspond well with the fact that the wt % of precursors added during the preparation was long enough for complete precipitation to occur.

Analysis of the catalyst via the X-ray diffraction (XRD) technique revealed that analyzing the chemical structure and crystallinity of the nickel oxide in the catalyst was not possible. Therefore, the compositions of the elements in both the AC catalyst and the Ni doped into the AC catalyst were determined via X-ray fluorescence (XRF) analysis and energy-dispersive X-ray fluorescence (EDXRF) to determine the composition and amount of trace elements present in the

https://doi.org/10.1021/acsomega.4c08111
ACS Omega 2025, 10, 14699−14722

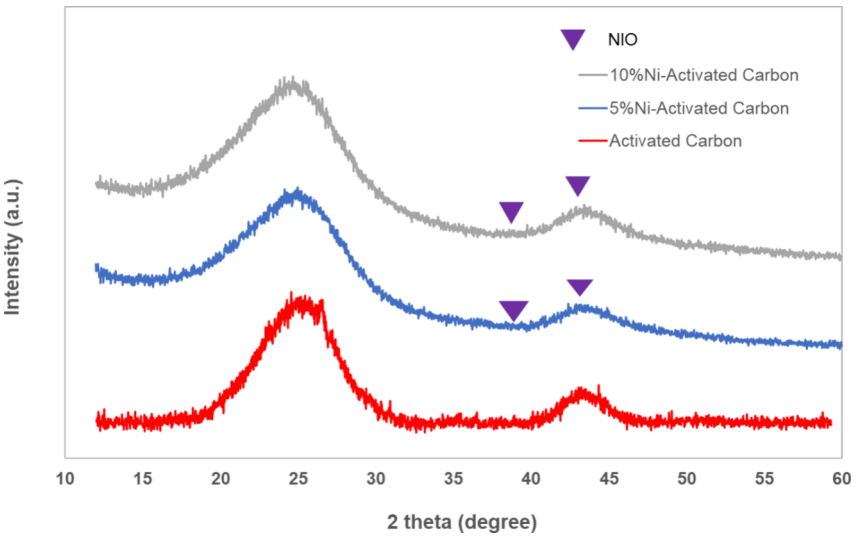

Figure 2. XRD analysis of activated carbon and several types of Ni doped over activated carbon.

catalyst. In Table 4, the XRF analysis confirmed the elemental composition of the activated carbon, which was mainly carbon

Table 4. XRF Analyses of Activated Carbon

element	oxide	concentration (wt %)
C		98.73
Na	Na_2O	0.42
Si	SiO_2	0.08
Ni	NiO	0.28
P	P_2O_5	0.04
K	K_2O	0.33
Ca	CaO	0.08
S	SO_3	0.03
Fe	Fe_2O_3	0.01

at 98.73 wt % and contained very small amounts of other elements found in the composition of the AC catalyst.

As shown in Table 5, the EDXRF confirmed the elemental composition, which implies the elemental oxide when 3 to 10

Table 5. EDX Analyses of the Oxide that Appeared after Ni Modification of the AC Catalyst

		concentration of Ni (wt %)		
element	oxide	3%Ni/AC	5%Ni/AC	10%Ni/AC
Ni	NiO	0.94	3.82	8.07

wt % Ni was impregnated into the parent AC support structure, which illustrated that the content of Ni metal consisted of a negligible percentage of Ni doped into the AC catalyst: only 0.94 wt % with 3 wt % Ni impregnated into the AC catalyst. An increase in the %Ni of the AC catalyst from 5 to 10 wt % resulted in Ni contents of 3.82 and 8.07 wt %, respectively. Notably, the weight percentage of NiO analyzed via EDXRF is also slightly different from that calculated via wet impregnation preparation into the AC support structure. This result shows that the prepared catalyst contains copper NiO in the desired proportion. However, XRD cannot clearly illustrate the analysis of NiO on AC supports via the XRD pattern because it may be highly dispersed or have a crystal size smaller than 2 nm. Therefore, EDXRF analysis confirmed the presence of NiO in the catalyst even when only a very small amount of Ni was present in the AC support template.

The textural structures of AC, 5 wt % Ni/AC, and 10 wt % Ni/AC were determined from the N_2 adsorption−desorption isotherms recorded on the AC and Ni impregnated with AC, which illustrated the porous structure, and the isotherms of the catalysts with the Ni precursors in the activated carbon template were determined via the BET technique to reveal the amount of nitrogen gas adsorbed on the surface of the catalyst.

Figure 3 shows the shape of the N_2 adsorption−desorption isotherm as an IV-type isothermal plot with an apparent

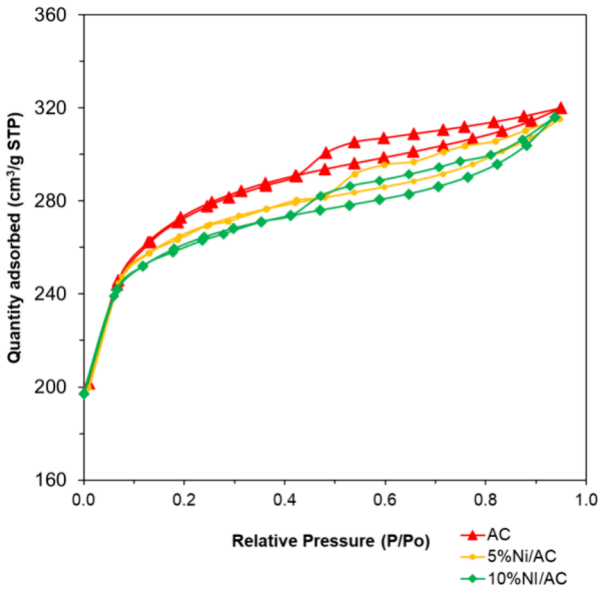

Figure 3. Adsorption−desorption isotherms determined via BET analyses.

hysteretic loop of the desorption branch,[25] revealing that many mesopores exist in the AC, which consists of partly micropores (<2 nm) and mainly mesopores (pore size of 2−50 nm), indicating that the AC contains a mesoporous structure. Additionally, the isotherm shown in Figure 3 indicates that the amount of adsorbed and desorbed gas is not equal at a relative pressure (P/P_0) of 0.42−0.96, which can contribute to

https://doi.org/10.1021/acsomega.4c08111
ACS Omega 2025, 10, 14699−14722

capillary condensation in the pores,[25,30] indicating the presence of many mesopores or pores between 2 and 50 nm.

The textural properties of the AC and Ni/AC samples obtained from the nitrogen sorption isotherms revealed the specific surface area, pore volume, and average pore size, as shown in Table 6. In general, AC has a high BET surface area,

Table 6. Textural Properties of Activated Carbon and Ni-Doped Activated Carbon

catalyst	BET surface area (m^2/g)	pore volume (cm^3/g)	average pore size (nm)
AC	1113.43	0.64	2.52
5%Ni/AC	962.84	0.56	3.35
10%Ni/AC	837.78	0.51	3.38

strongly acidic active sites, large total pore volume, and uniform meso-porosity including a small proportion of micropores, which indeed serve as catalysts in aromatization reactions. The porosity of a catalyst strongly influences its catalytic activity,[25,30] which usually enhance the delivery of the catalytic process to the reactants. The modification of the parent AC support with a metal oxide affected the pore structure and pore size distribution, resulting in the formation of more mesoporous and micropore structures but a slight change in the specific surface area of the AC. The small crystallites of NiO might be derived from the rate of nucleation being greater than the rate of increase in the number of nuclei with increasing content of modified Ni to the AC parent template, corresponding to the gradually increasing Ni loading, resulting in a slight increase in the crystallite size and a gradual decrease in the surface area.

Table 6 shows the specific surface area and porosity of both the activated carbon catalyst and the Ni doped on the AC catalyst from 5 to 10 wt % NiO showed that the AC catalyst has a specific surface area of 1113.43 m^2/g, a pore volume of 0.64 cm^3/g, and an average pore size of 2.22 nm. Furthermore, the acid strength of a catalyst's support affects the supporting properties upon the modification of catalyst preparation by an impregnation technique. However, the acidity of Ni/AC via the TPD-NH_3 technique was not investigated due to instrument limitations. When the Ni was impregnated into the parent activated carbon with nickel nitrate at concentrations ranging from 5 to 10 wt %, the specific surface area and pore volume were reduced, while the pore size increased. To determine the specific surface area and porosity of the modified Ni, different concentrations of NiO were incorporated into AC. Notably, as the NiO concentration increased, the specific surface area of the catalyst also decreased. The 5 wt % Ni/AC catalyst has a specific surface area of 962.84 m^2/g, a pore volume of 0.56 cm^3/g, a pore size of 3.35 nm, while the 10 wt % Ni/AC catalyst had a specific surface area of 837.78 m^2/g, a pore volume of 0.51 cm^3/g, and a pore size of 3.38 nm. The decrease in specific surface area is caused by NiO particles, which have a small specific surface area, covering the surface of the parent activated carbon, thus reducing the specific surface area of the parent activated carbon catalyst. Additionally, the average pore size is a key parameter affecting the surface area. A catalyst with large pores tends to have a specific surface area. However, if the pores are small, then the specific surface area increases, which is in line with the impregnated catalyst with 10 wt % of NiO added to the parent activated carbon.

3.3. Effect of Operating Conditions on the Product Distribution of Pyrolysis Oil. *3.3.1. Influence of Temperature.* Temperature is an important influencing parameter in the thermal decomposition reaction of both raw materials during the pyrolysis process. In particular, increasing the operating temperature accelerated the deoxygenation reaction in UCO through decarbonylation and fatty acid triglycerides, diglycerides, and monoglycerides, after which the carboxylation of fatty acids resulted in middle aliphatic hydrocarbons and further decomposed into a smaller hydrocarbon chain and continued to enhance the bond cleavage of C−C and C−H bonds from thermal degradation into free radicals until it arranged and formulated a medium-sized hydrocarbon chain.

Moreover, ULO can undergo thermal decomposition, are thermally stable, and contain a certain proportion of hydrogen. Therefore, the thermal decomposition of ULO enhanced the bond cleavage of C−C and C−H bonds into a shorter hydrocarbon chain. Additionally, thermal decomposition affects the co-occurrence of noncondensable gases such as CO, CH_4, C_2H_4, and H_2 via copyrolysis reactions.[9,15]

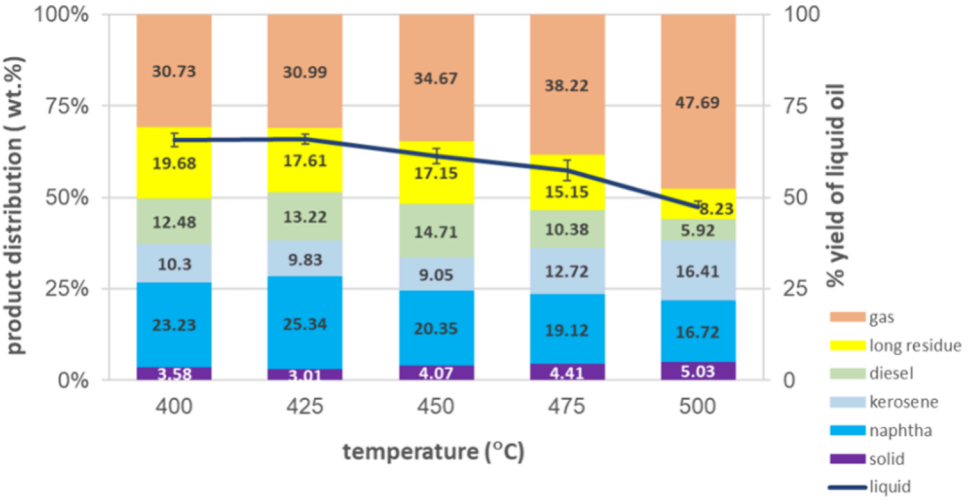

Figure 4. Effect of temperature on the product distribution at an inert N_2 flow rate of 50 mL/min with a 0.5/0.5 mass molar ratio of ULO/UCO, 5 wt % Ni doped on activated carbon catalyst by using 5 wt % catalyst loading into the cofeedstock.

https://doi.org/10.1021/acsomega.4c08111
ACS Omega 2025, 10, 14699−14722

Figure 4 shows the product yield and distribution obtained through copyrolysis by varying the process temperature from 400 to 500 °C. The product distribution was performed with a ULO/UCO mass ratio of 0.5/0.5 at a constant N_2 flow rate of 50 mL/min over 5 wt % Ni-doped AC catalyst and 5 wt % catalyst loading to the feedstock.

As the temperature increased from 400 to 500 °C, the liquid yield slightly changed to approximately 65.69 ± 1.83 and 66.00 ± 1.36 wt % as the temperature increased from 400 to 425 °C and then decreased to 61.26 ± 2.04 wt % at a pyrolysis temperature of 450 °C. When the pyrolysis temperature was greater than 475 °C, the yield of the liquid product dramatically increased from 57.37 ± 2.83 to 47.28 ± 1.77 wt %. The highest liquid yield was 66.00 ± 1.36 wt % at 425 °C, whereas when the temperature was increased to 500 °C, the percentage yield of the liquid product tended to decrease to 47.28 ± 1.77 wt %, and the highest yield of noncondensable gases of 47.69 ± 0.49 wt % was obtained. When the pyrolysis temperature increases, it affects the rate of reaction through thermal degradation due to an endothermic reaction and also plays a crucial role in the bond cleavage of both the ULO and UCO to contribute both free radicals and hydrocarbon radicals, which continues to increase the bond scission of C−C and C−H from large-chain hydrocarbon compounds into smaller-chain compounds.[6,9] When increasing the temperature in catalytic copyrolysis, the effect of the acid strength on the large surface area, including the porosity of activated carbon catalyst, enhances the C−C bond cleavage and results in the formation of small hydrocarbon compounds by reacting with the Ni active site and mesopores of the AC catalyst. Then, further cracking reaction occurs via bond scission and hydrogen transfer on the surface of the Ni/AC catalyst, where the acid strength from the Ni-doped AC catalyst increases to promote the β-scission of the C−C bond, resulting in the occurrence of small hydrocarbon chains,[17,25,29] whereas the influence of the mesopores and large surface area on AC allows the formation of hydrocarbon compounds through catalytic copyrolysis into light hydrocarbons with 5−15 atoms in the naphtha-like fraction and kerosene-like fraction, respectively.[17,25] After that, the further cracking of smaller hydrocarbon compounds continued, resulting in cracking into noncondensable gases and small hydrocarbon gases. In addition, increasing the copyrolysis temperature slightly decreased the %yield of liquid when the temperature increased from 400 to 450 °C and dramatically decreased to 47.28 ± 1.77% when the temperature was increased to 500 °C. However, notably, as the copyrolysis temperature increased from 400 to 500 °C, the gas yield increased from 30.73 ± 1.13 to 47.69 ± 0.49 wt %, whereas the %yield of the solid product slightly increased from 3.58 ± 0.52 to 5.03 ± 1.85 wt % as the copyrolysis temperature increased with respect to the temperature, as shown in Figure 4.

The product distribution of the liquid fraction was analyzed in accordance with the boiling temperature with a gas chromatograph to simulate distillation, according to ASTM D86. The yield percentage of the product distribution according to the naphtha-like fraction tends to increase from 23.23 to 25.34 wt % when the operating temperature increases from 400 to 425 °C and clearly tends to decrease when the pyrolysis temperature increases from 450 °C (20.35 wt %) to 475 °C (16.72 wt %). The results of the copyrolysis reaction and analyses of a simulated distillation gas chromatograph correspond to the increasing occurrence trend of noncondensable gases, which can indicate that the effects of thermal decomposition and decomposition with a catalyst that contains strong acid active sites, including the influence of pore-selective properties, cause the decomposition of medium to small hydrocarbon chains and the formation of a large amount of several noncondensable hydrocarbon gases when the operating temperature is increased, while the influence of high temperature is also strongly dominant, resulting in the secondary cracking reaction of volatile vapors to obtain a large amount of a noncondensable gas yield. In addition, the results also indicate that the occurrence of large hydrocarbons in the C_{15}−C_{19}+ range from the deoxygenation of ULO/UCO at low temperatures and the thermal stability of ULO promote the decarbonylation and decarboxylation of large hydrocarbon compounds and the removal of CO and CO_2, respectively.[9,38] When the temperature increased, large hydrocarbon chains continued to decompose under the influence of a high temperature, causing the random breakdown of chains into free radicals and resulting in smaller hydrocarbons. Then, the catalyst played a role in catalyzing the cracking reaction to break down C−C and C−H bonds, yielding hydrocarbon compounds with kerosene-like properties (carbon numbers between C_{11} and C_{15}). Consequently, increasing the pyrolysis temperature above 450 °C enhances the kerosene-like fraction.

However, increasing the pyrolysis temperature tends to accelerate the thermal cracking of large hydrocarbon chains, ranging from C_{19} to C_{33}+, which continues to crack via thermal decomposition. Both C−H and C−C bond cleavage by free radicals and hydrocarbon radicals,[9,15,17,18] bond scission and structural reforming at the acid active site, and the pore-selective properties of the catalyst to obtain smaller hydrocarbon chains tend to decrease the diesel-like fraction. The operating temperature enhances the degradation of large chains into smaller hydrocarbon compounds, and the effect of high temperature also induces the secondary cracking reaction of volatile vapor to noncondensable gas, as the %yield of noncondensable products greatly increases from 30.73 to 47.69 wt % as the copyrolysis temperature increases with respect to the temperature, as shown in Figure 4.

3.3.2. Influence of Inert N_2 Carrier Gas. The nitrogen gas flow rate is an important parameter in the pyrolysis process because nitrogen gas plays a role in both facilitating devolatilization to obtain volatile vapor that occurs from the thermal decomposition of large hydrocarbon chains at the pyrolysis operating temperature and is an inert carrier gas of volatile vapor from the reactor to the condensation unit. Therefore, the flow rate of nitrogen gas is related to the residence time of the reaction, which often has a significant effect on the thermal cracking. In the early state of thermal cracking, the temperature plays an important role in the breakdown of triglyceride and fatty acid molecules into medium-sized hydrocarbon chains. Moreover, an inert N_2 atmosphere increases the number of cleaved C−O bonds, C−O bonds, C−C bonds, and C−H bonds of fatty acids through decarbonylation and decarboxylation reactions. These phenomena contribute to the formation of small hydrocarbon compounds and noncondensable gases. The nitrogen gas atmosphere in the reactor also generates conditions for pyrolysis in the absence of oxygen and enhances the deoxygenation of UCO to fatty acids, which decompose by decarbonylation and decarboxylation reactions to produce CO and CO_2.[17,18,24,26,38] Therefore, the nitrogen flow rate plays a crucial role in both increasing the residence time for thermal

https://doi.org/10.1021/acsomega.4c08111
ACS Omega 2025, 10, 14699−14722

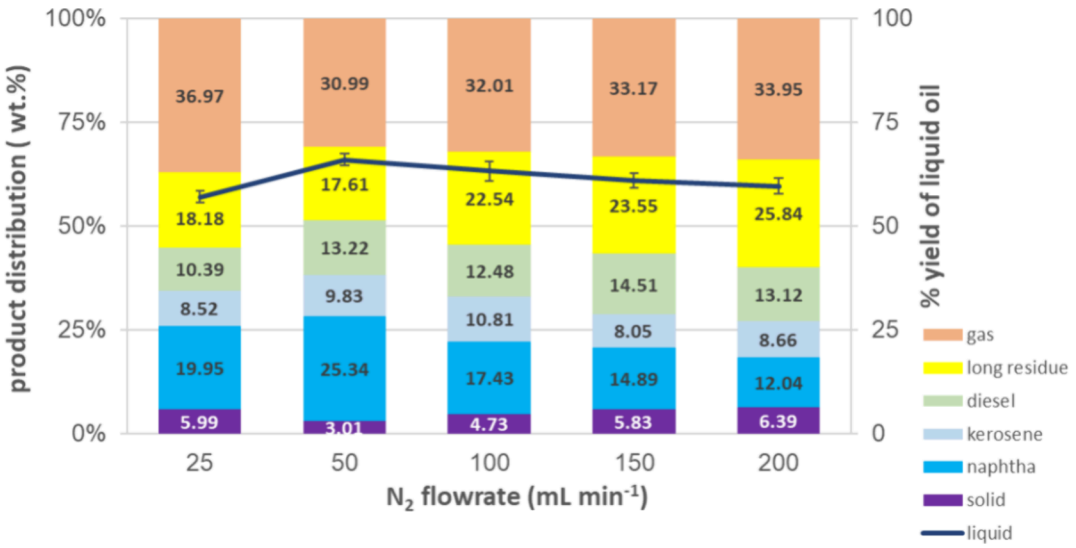

Figure 5. Effect of the N_2 flow rate on the product distribution at an operating temperature of 425 °C at a 0.5/0.5 mass molar ratio of ULO/UCO and 5 wt % Ni doped on activated carbon catalyst by using 5 wt % catalyst loading into the cofeedstock.

disintegration and enhancing the promotion of deoxygenation reactions. Then, medium-sized hydrocarbons undergo a radical splitting reaction, causing C−H bond cleavage and C−C bond cleavage, which results in smaller hydrocarbon compounds.[26,38]

Moreover, hydrogen is also produced from the thermal decomposition of free radicals, and hydrocarbon radicals undergo a hydrogen transfer reaction, causing cleavage of the medium-sized hydrocarbon to smaller hydrocarbons at the β-position of the hydrocarbon chain resulting in the formation of aliphatic hydrocarbons that become saturated linear aliphatic hydrocarbon compounds.

The Ni/AC-catalyzed cracking reaction can promote hydrocarbon cracking to properly obtain volatile vapor from NiO, which has a strong acid active site over the AC template at a low flow rate of inert nitrogen, affecting the pyrolysis reaction of ULO/UCO to continue breaking down the C−C bond, which has a longer residence time of reaction coupled with catalytic cracking, which may cause a hydrogenation reaction resulting from the formation of hydrogen gas under an atmosphere of inert N_2 gas, resulting in the occurrence of medium hydrocarbon compounds and further breakdown into smaller hydrocarbons such as saturated straight aliphatic hydrocarbon compounds by hydrogenation to the C═C bond that occurs from thermal degradation and C−C bond cleavage.[34,35,41] Furthermore, the nitrogen gas flow rate is related to the residence time of the pyrolysis reaction within the reactor and has a great influence on thermal degradation and catalytic pyrolysis, which increase the degree of C−C bond and C−H bond scission, causing volatile vapor inside the reactor during the pyrolysis process.

At a low flow rate of inert nitrogen gas, the thermal cracking reaction had a greater effect on volatile vapor formation than catalytic cracking; this led to breakdown of hydrocarbons into smaller molecules and further secondary cracking reactions to decompose them by breaking down into hydrocarbon gases and noncondensable gases, resulting in a decrease in the yield of liquid products, while a large amount of noncondensable gases was observed. However, a nitrogen flow rate of 50 mL/min produced the highest percentage yield of liquid product of 66.00 ± 1.36 wt % and obtained the highest percentage of naphtha-like fraction of 25.34 wt %, respectively.

Figure 5 shows the trends in the product yield and the distribution product during the catalytic copyrolysis of the ULO and UCO when the flow rate of inert nitrogen gas fed into the pyrolysis reactor was varied under the following conditions: a temperature of 425 °C, 5 wt % Ni-doped AC by using the 5 wt % catalyst loading to feedstocks, and a 0.5:0.5 mass molar ratio of ULO/UCO. Notably, the cofeedstock underwent catalytic copyrolysis at a high flow rate of inert N_2 fed into the reactor (200 mL/min), presented the yield percentage of liquid product of 59.66 ± 1.84 wt %, and only consisted of 12.04 wt % of naphtha-like fractions that are very small, whereas the fraction similar to kerosene was not very high because the pyrolysis and heat transfer from the reactor wall to the feedstock are not sufficient to properly crack the large hydrocarbon chains. Instead, the volatile vapor of the large hydrocarbon chains was gassed by the high flow rate of nitrogen carrier gas and rapidly passed through the reactor to the condensation unit without proper thermal cracking.

When the flow rate of the nitrogen carrier gas was reduced from 150 to 50 mL/min, the liquid yield tended to increase from 61.00 ± 1.76 to 66.00 ± 1.36 wt %, the naphtha-like fraction also tended to increase from 12.04 to 25.34 wt %, and the gas products decreased only slightly from 33.95 ± 2.03 to 30.99 ± 1.45 wt %, whereas the solid char formation tended to decrease from 6.39 ± 0.57 to 3.01 ± 1.34 wt % and increased to 5.99 ± 0.68 wt % when the N_2 flow rate was reduced to 25 mL/min. This can be explained by the fact that high temperatures have a great effect on thermal cracking. At the initial stage, an increased temperature plays a crucial role in the cracking of triglyceride fatty acid into medium hydrocarbon chains. Moreover, the temperature enhances the decomposition of C−H and C−C bonds in fatty acids through a decarboxylation reaction. When a nitrogen flow rate is not too high, volatile vapor and medium hydrocarbon chains break down into smaller molecules, and further β-scission bond cleavage and structural rearrangement occur though the pore-selective properties and textural structure of the activated carbon support template.[11,18,21]

https://doi.org/10.1021/acsomega.4c08111
ACS Omega 2025, 10, 14699−14722

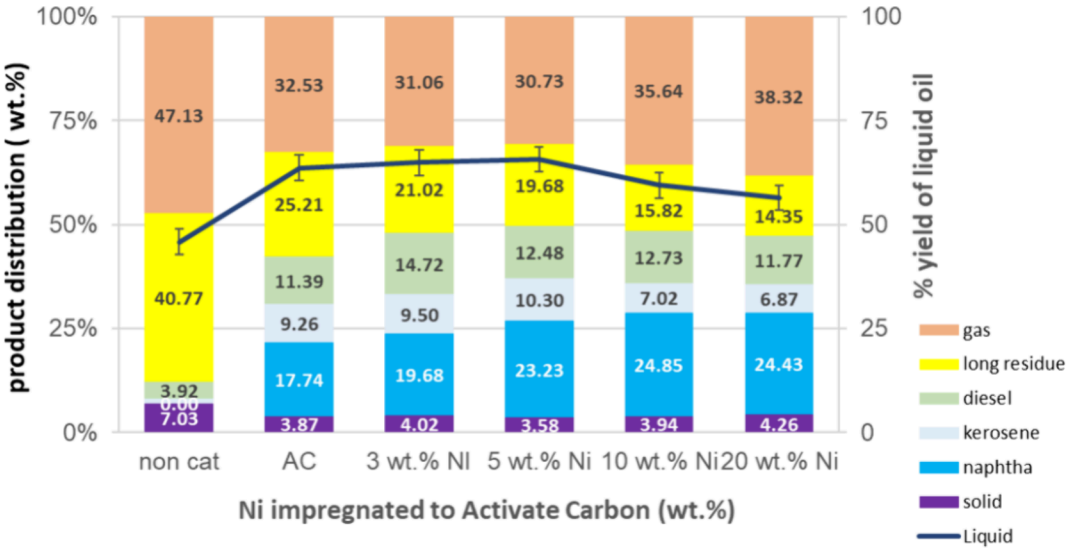

Figure 6. Effect of the weight percentage of Ni doped on the activated carbon catalyst on the product distribution at an operating temperature of 425 °C, an inert N_2 flow rate of 50 mL/min, and a 0.5/0.5 mass molar ratio of ULO/UCO by using 5 wt % catalyst loading into the cofeedstock.

It was also observed that the product distribution of the naphtha-like fractions increased at the high residence time due to the fact that the effect of heat transfer in the pyrolysis reactor promoted the breakdown of the medium and therefore accelerated its cleavage of C−C bonds to small hydrocarbon chains. The residence time is high, causing the UCO that undergoes thermal decomposition to have a suitable hydrocarbon radical that promotes the thermal cracking of the ULO and reduces its thermal stability,[9,15] resulting in thermal cracking, catalytic cracking reactions, and secondary cracking until large hydrocarbon molecules break down into smaller hydrocarbon molecules, such as naphtha-like and kerosene-like fractions, and several compositions of hydrocarbon gases are observed.

3.3.3. Influence of wt % Ni Modification on Activated Carbon. The modification of the metal in the AC catalyst effectively improved the catalytic activity during copyrolysis, resulting in increased strength of the acidic active sites, improved porosity, and an increased number of interlayers in the AC catalyst. The effect of Ni doping on the catalytic activity on the product distribution from copyrolysis of 0.5/0.5 mass molar ratios of ULO/UCO when the operating temperature was held constant at 425 °C, an inert N_2 carrier at 50 mL/min, and 5 wt % catalyst loading into the cofeedstocks was observed. The product distribution of the copyrolysis of ULO/UCO was determined via the use of activated carbon with various amounts of Ni impregnated into the AC support template, as illustrated in Figure 6. The results revealed that, compared with the use of a catalyst, the thermal degradation of ULO/UCO alone resulted in the highest percentage of a solid yield of 7.03 ± 1.02 wt % compared with the use of a catalyst; the percentage of a solid yield was approximately 3.87 ± 0.92 to 4.26 ± 1.75 wt %.

In addition, the occurrence of the naphtha-like fraction, kerosene-like fraction, and diesel-like fraction was also less abundant than in the catalytic pyrolysis, which can be explained by the fact that the thermal decomposition of ULO/UCO involves the random bond cleavage of large hydrocarbon chains with an increased temperature, which is also initially affected to promote the decarbonylation and decarboxylation of UCO to fatty acids to obtain CO and CO_2,[9,15] whereas the influence of the increased temperature promotes randomized bond cleavage in the form of free radical and hydrocarbon radical for continually cracking of the large hydrocarbon chain to smaller chains.[17,18]

The process conditions at high temperatures and long residence times therefore accrue the cleavage of small chains to noncondensable gases and promote the degradation of the ULO, which also has greater thermal stability. Therefore, the long residue fraction was 40.77 wt % due to depolymerization and the termination of the radical reaction. Comparison of the effects of catalytic copyrolysis using only AC and the Ni-doped AC catalyst on the product distribution revealed that the liquid product was obtained at 63.60 ± 2.83 wt % when it was catalyzed with AC, whereas the liquid yield slightly increased from 64.92 ± 2.28 to 65.69 ± 2.22 wt % with increasing Ni doping to the AC catalyst from 3 to 5 wt % of doped Ni, and the liquid yield decreased to 59.42 ± 1.02 and 56.42 ± 1.65 wt % as the Ni doping increased to 10 and 20 wt %, respectively. Furthermore, it is worth noting that the yield of noncondensable gas has a trend similar to that of the pyrolytic oil yield obtained from catalytic copyrolysis with increasing Ni loading into the AC catalyst.

Notably, when the amount of Ni doped with the AC catalyst was increased to 10 and 20 wt %, the yield percentage of the liquid product decreased to 59.42 ± 1.02 and 56.42 ± 1.65 wt %, whereas the yield percentage of noncondensable gas also increased significantly to 35.64 ± 1.73 and 38.32 ± 2.22 wt %, respectively, which is described by an increase in the wt % of Ni doped on the AC catalyst, increasing the dispersion of the Ni active site, which also has strong acidity active sites on the AC support template, promoting the breakage of C−C bonds from medium−hydrocarbon chains to small hydrocarbon chains;[7,29,35] thus, the influence of operating conditions at high temperature plays a crucial role in the continuous cracking of light hydrocarbon molecules (C_5−C_8), including secondary cracking reactions that result in the production of light hydrocarbon compounds that break down to smaller and further cracking into the C_2−C_4 hydrocarbon gas.[30,34,35] Notably, the catalytic activity of the Ni-doped AC catalyst and only the AC catalyst alone slightly changed the liquid product yield from the catalytic copyrolysis of ULO/UCO,

https://doi.org/10.1021/acsomega.4c08111
ACS Omega 2025, 10, 14699−14722

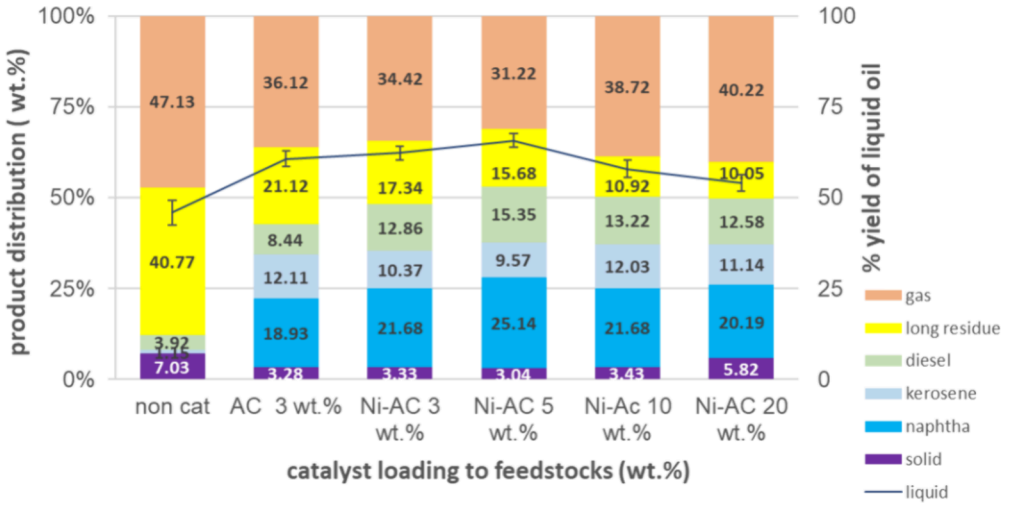

Figure 7. Effect of the percentage of catalyst loading to cofeedstock on the product distribution at an operating temperature of 450 °C, an inert N_2 flow rate of 50 mL/min, a 0.5/0.5 mass molar ULO/UCO ratio, and 5 wt % Ni doped on the activated carbon catalyst.

whereas the analyses of product distribution via a simulated distillation gas chromatograph according to ASTM D86 revealed a significant difference in yield percentages of the product distribution. The products obtained from the catalytic copyrolysis of ULO/UCO with an individual AC catalyst consisted of 17.74, 9.26, 11.39, and 25.21 wt % of naphtha-like, kerosene-like, diesel-like, and long residue fractions, respectively. Moreover, an increased Ni concentration in the AC catalyst contributed to the formation of high-strength acidic active sites, which enhanced the C−C bond cleavage in small hydrocarbon compounds and facilitated the rearrangement of medium hydrocarbon molecules through mesopores and H-transfer over the active sites, breaking down medium hydrocarbon chains into smaller compounds. Additionally, hydrogenation increased the number of saturated hydrocarbon compounds,[18,30,38] resulting in an increase in the naphtha-like fraction from 19.68 to 24.85 wt % when the Ni-doped concentration was increased from 3 to 10 wt %.

However, as the amount of Ni doped into the AC catalyst increased to 20 wt %, there was a slight decrease or almost no significant change in the yield percentage of the naphtha-like fraction (24.43 wt %); however, there was an increase in the yield percentage of noncondensable gas, 38.32 ± 2.22 wt %. Moreover, the product distribution in the kerosene-like, diesel-like, and long-residue fractions was lower than that in the catalytic copyrolysis of ULO/UCO using 10 wt % Ni/AC. This result indicates that the role of NiO on the AC catalyst accelerated the C−C bond cleavage because of the acidic active site on the AC support.[7,29] The role of the Ni/AC catalyst in reducing the activation energy of the reaction and the rate of formation of β-scission in a medium hydrocarbon chain and in breaking down the C−C bond through the AC catalyst was promoted owing to an increase in the strength of the acidic active site; then, the role of the porosity structure of AC affected the rearrangement of smaller hydrocarbon chains through the mesopore and large surface structure with a high pore volume to form a straight aliphatic hydrocarbon chain in the range of C_5−C_{19}.[18,30,33,38] The occurrence of volatile vapor from the thermal cracking of both ULO and UCO also continually cracked and could be formulated into suitable light hydrocarbon compounds established at lower concentrations of Ni doped on the AC catalyst, whereas the strength of the acidic active sites of AC tended to increase with the modification of the Ni to AC catalyst. Therefore, the medium-strength hydrocarbon chains are also reduced by the β-scission of C−C bonds by the Ni active site, and the secondary cracking of volatile vapors also results in the formation of small-molecule volatiles that can pass through and restructure inside the pores selectively[18], isomerization, cyclization, hydrogenation,[33] and oligomerization of condensable volatile vapors to increase the liquid yield,[33,38] which contains mostly the naphtha-like fraction.

When the amount of Ni doped on the AC catalyst increased even further, although the effect of the acidic active site from NiO accelerated the β-scission, resulting in the cleavage of the C−C of the hydrocarbon compounds into small hydrocarbon chains, the yield percentage of the liquid product and product distribution according to the desired aliphatic alkane in the carbon ranging from C_{12} to C_{18} exhibited the opposite trend when the amount of Ni doped on the AC catalyst was moderately increased. This finding could be attributed to the influence that the small crystallites of NiO might be derived from the rate of nucleation being greater than the rate of increase in the number of nuclei with increasing content of modified Ni to the AC parent template,[27,29] corresponding to the gradually increasing Ni loading, resulting in a slight increase in the crystallite size and a gradual decrease in the surface area; the catalyst channels were blocked by the high concentration of Ni doped, which significantly decreased the surface area, and the catalytic channel was blocked by the high concentration of Ni doped into the AC catalyst,[34,35,41] resulting in a decrease in catalytic activity. This led to a carbonaceous material being formulated at the acid active site by the depolymerization reaction and a further secondary cracking reaction. Therefore, the desired straight aliphatic hydrocarbon content moderately decreased with increasing addition of noncondensable gas from the influence of thermal cracking, which underwent thermal cracking, because the effect of the temperature was greater than that of the catalytic cracking reaction. The high loading of Ni to the AC support template may not be beneficial for the catalytic cracking of the ULO/UCO on the liquid yield and its desirable product distribution in the straight aliphatic compound in the carbon range of C_5−C_{11}. The analyses of the product distribution

https://doi.org/10.1021/acsomega.4c08111
ACS Omega 2025, 10, 14699−14722

revealed that the parameters and operating conditions for the catalytic copyrolysis of ULO/UCO with 5 wt % Ni doped on the AC catalyst resulted in the highest percentage of liquid yield (65.59 ± 2.22 wt %) and naphtha-like fraction (23.23 wt %), which was insignificantly different from the 10 wt % Ni doped into the AC catalyst.

3.3.4. Influence of the Mass of the Catalyst on the Cofeedstock. As shown in Figure 7, the influence of catalyst loading to feedstock on the yield percentage and product distribution obtained from copyrolysis of ULO/UCO at a 0.5:0.5 mass ratio by the operating condition of 425 °C, an inert N_2 flow rate of 50 mL/min, and 5 wt % Ni doped on AC catalysts illustrated the comparison between the thermal cracking and catalytic cracking of the cofeedstock. The yield percentage of noncondensable gas was extremely high yield at 47.13 wt %, and notably, the highest percentage of solid yield of 7.03 wt % was obtained compared with that of copyrolysis using a catalyst, which resulted in the yield percentage of noncondensable gas and solid of approximately 31.22−36.12 and 3.04−5.82 wt %, respectively. The naphtha-like fraction, kerosene-like fraction, and diesel-like fraction are also less abundant than they are in catalytic pyrolysis, whereas the percentage yield of long residue from noncatalytic pyrolysis was 40.77 wt %.

This indicates that the thermal degradation during copyrolysis involved the randomized bond cleavage of large hydrocarbon chains when the temperature was initially increased to promote the decarbonylation and decarboxylation of UCO into fatty acids to the formation of CO and CO_2.[4] Subsequently, the effect of temperature involved the randomized decomposition of C−H bonds and C−H bonds into free radicals, probably because the hydrocarbon radicals from both the ULO and UCO underwent a reaction to C−C bond cleavage and obviously formed, forming smaller hydrocarbons, while the secondary cracking reaction at high temperatures also accelerated the conversion of small condensable volatile vapors to noncondensable gases.

The catalytic copyrolysis reaction using an AC catalyst at 3 wt % loading into the feedstock was performed under the same conditions as those used for noncatalytic cracking. The catalytic activity of the AC catalyst with 3 wt % loading into the feedstock resulted in the yield percentage of liquid of approximately 60.60 ± 2.75 wt %, and the yield percentages of noncondensable gas and solid decreased to 36.12 ± 1.03 and 3.28 ± 0.94 wt %, respectively. Additionally, the analyses of product distribution revealed a significant increase in the naphtha-like, kerosene-like, and diesel-like products to 18.93, 12.11, and 8.44 wt %, respectively, while the long residue fraction was only 21.12 wt %. This finding revealed that the thermal decomposition of ULO/UCO occurred since the increased temperature also initially affected the carbonylation and carboxylation of UCO, followed by the randomized bond cleavage of the large hydrocarbon chains into hydrogen radicals and hydrocarbon radicals to the formation of middle hydrocarbon chains, whereas high temperatures also reduced the thermal stability of the ULO, resulting in enhanced cleavage of the C−C bonds from both the ULO and UCO into middle hydrocarbon chains.[9,17,18] The catalytic activity may be attributed to the fact that the catalyst provided strong acidic activated sites, accelerating hydrogen transfer though β-scission, and the cleavage of C−C bonds accelerated the decomposition of middle hydrocarbon compounds and the formation of straight hydrocarbon compounds.[23,34,35,41] Moreover, the AC catalyst has a large pore volume and high surface area, which promote the selectivity of condensable volatiles to form straight aliphatic hydrocarbons in the C_5−C_{11} range. Therefore, the product distribution of liquid pyrolysis oil also consisted of the C_7−C_{16} range. Notably, the yield percentage of long residue decreased to 21.21 wt % compared to that obtained from the copyrolysis of ULO/UCO without the AC catalyst, which was influenced by the catalytic activity of the strong acidic active site. This increase in yield increased the β-scission of C−C bonds into small hydrocarbon compounds. Then, the textural structure of the AC catalyst, such as its large surface area, high pore volume, and pore selectivity, cracked and cracked and rearranged the condensable volatile vapor to formulate the properly aliphatic hydrocarbon compounds in C_8−C_{19}, resulting in the occurrence of diesel-like, kerosene-like, and naphtha-like fractions.

Compared with the resulting product distribution derived from the catalytic copyrolysis of ULO/UCO at a 0.5:0.5 mass ratio under the operating condition of 425 °C, with an inert N_2 flow rate of 50 mL/min by using the 3 wt % individual AC catalyst loading into feedstocks and the product distributions of the solid yield (3.33 wt %) and gas yield (34.42 wt %), the naphtha-like and diesel-like fractions increased to 21.68 and 12.86 wt %, respectively, when 3 wt % loading with 5 wt % Ni doped on the AC catalyst was employed.

The effects of catalyst loading into feedstock in the catalytic copyrolysis of ULO/UCO at a 0.5:0.5 mass ratio at an operating condition of 425 °C and an inert N_2 flow rate of 50 mL/min using 5 wt % Ni doped into AC catalysts on the product distribution were investigated by varying the catalyst loading ratio to feedstock. The rate of the catalytic copyrolysis reaction may be correlated with the catalyst loading, which is related to the increase in the number of active sites on the catalyst. Increasing the catalyst loading to 5 wt % increased the catalytic activity of both the strength acidic active site and the pore-selective property during the cracking reaction, resulting in the catalytic activity of the volatiles and increasing the amount of copyrolysis oil to 65.74 ± 0.71 wt %. The amounts of diesel-like fraction (15.35 wt %) and naphtha-like fraction (25.14 wt %) significantly increased. The yield percentage of carbonaceous material rarely significantly changed (approximately 3 wt %) when the catalyst loading was increased from 5 to 10 wt %. While the catalyst loading was increased to 10 and 20 wt %, the percentages of liquid, naphtha-like, kerosene-like, diesel-like, and long residues significantly decreased. In contrast, the content of noncondensable gas dramatically increased to 38.72 ± 1.74 and 40.22 ± 1.89 wt %.

The results were consistent with the strength of the acidic active site on the surface structure and textural properties of the Ni/AC catalyst, which increased with higher catalyst loading during copyrrolyzation under mild operating conditions (425 °C, inert N_2 flow of 50 mL/min). This affected the conversion of medium volatile vapor produced from the thermal degradation of both ULO/UCO, which correspondingly passed through the strong acidic active site and pore structure of the Ni/AC catalyst. As a result, successive degradation led to the formulation of short-molecule hydrocarbons, and the interaction between the catalyst, which contained a large amount of acidic active sites, accelerated the C−C bond cleavage, which facilitated the formation of small hydrocarbon compounds, whereas the copyrolysis reaction, which involved high temperatures and long residence times, promoted the conversion of small volatile vapors and

https://doi.org/10.1021/acsomega.4c08111
ACS Omega 2025, 10, 14699−14722

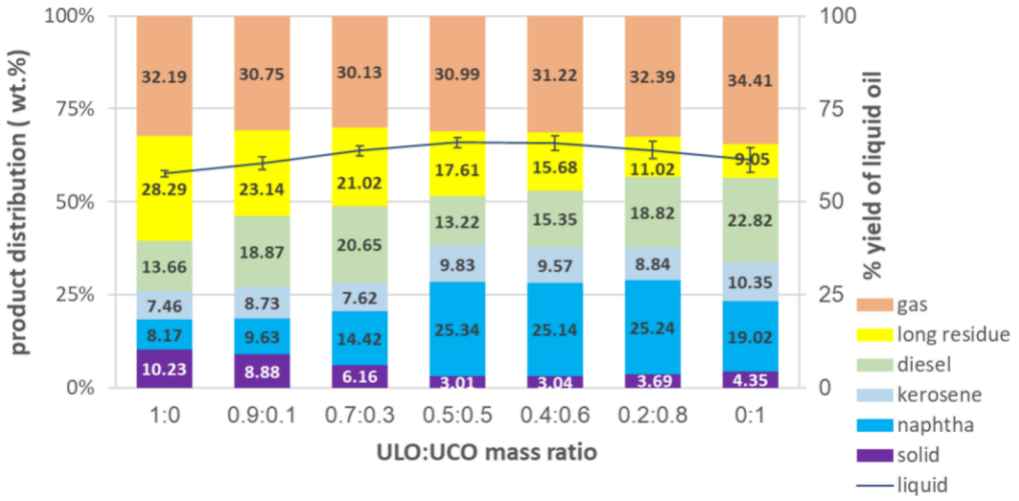

Figure 8. Effects of the mass molar ratio of the ULO/UCO on the product distribution at an operating temperature of 425 °C, an inert N_2 flow rate of 50 mL/min, and 5 wt % Ni doped on activated carbon catalyst by using 5 wt % catalyst loading.

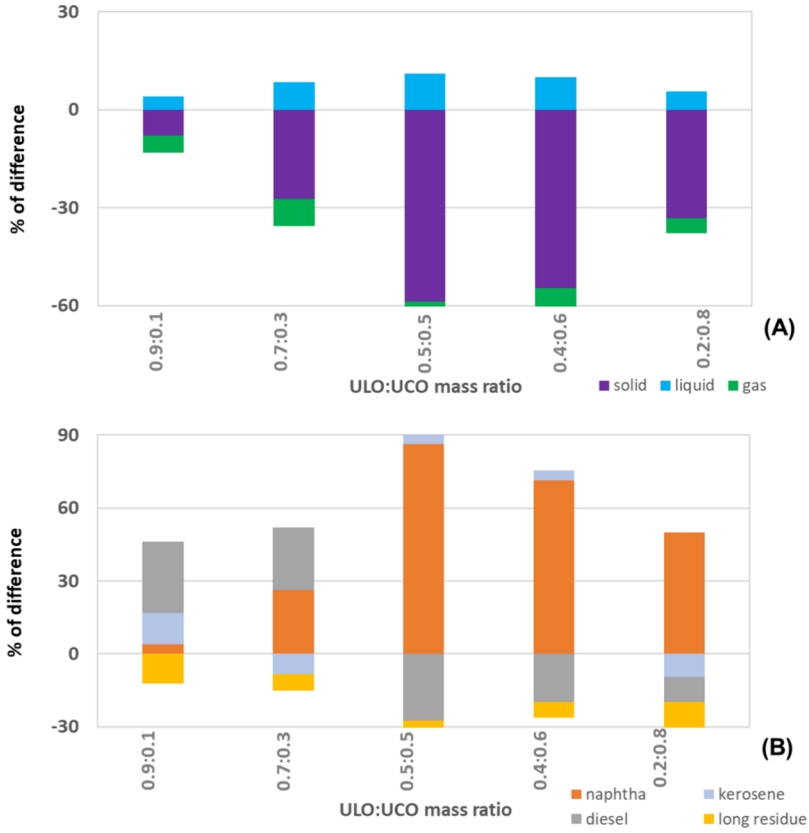

Figure 9. Synergy of the ULO/ULO mass molar ratio through catalytic copyrolysis at an operating temperature of 425 °C, an inert N_2 flow rate of 50 mL/min, and 5 wt % Ni doped on activated carbon by using 5% catalyst loading: (A) % difference in yield and (B) % difference in product distribution.

continually cracked volatile vapors into obviously the production of noncondensable gases.[9,15] Furthermore, the yield of solid char increased to 3.43 ± 1.15 and 5.82 ± 0.77 wt % when the catalyst loading was from 10 to 20 wt %, revealing that the active sites on the catalyst collapsed and aggregated, resulting in reduced catalytic activity. Some of the long-chain hydrocarbons were unable to enter the pores to undergo C−C bond breaking, and a significant amount of carbonaceous material accumulated at the acidic active sites, while the presence of carbonaceous deposits may have resulted in a reduction in the surface area and pore blockage of the catalyst affecting the catalytic performance was also deactivated.[7,31] After that, only the thermal cracking of the large hydrocarbon chains from the copyrolysis of the ULO/UCO feedstocks produced intermediate volatile compounds, while the influence of the high operating temperature continuously enhanced the decomposition of the C−C bond cleavage of the middle condensable volatile vapor to a smaller hydrocarbon vapor and was further influenced by the high temperature, which enhanced the secondary cracking reaction that continually

https://doi.org/10.1021/acsomega.4c08111
ACS Omega 2025, 10, 14699−14722

cracked them to produce a large amount of noncondensable gas, leading to the repolymerization of small hydrocarbons to produce noncondensable gas.[26] Therefore, excessive catalyst loading in the copyrolysis of ULO/UCO is not beneficial for fuel-like production within the carbon range of C_5-C_{19}, as it increases the level of noncondensable gas formation.

3.3.5. Influence of the ULO/UCO Mass Ratio. The effects of a blend ULO/UCO ratio ranging from 0.9:0.1 to 0.2:0.8 on catalytic copyrolysis at an operating condition of 425 °C, an inert N_2 flow rate of 50 mL/min, and 5%Ni/AC by using 5 wt % catalyst loading were investigated, and the results were compared with those of the catalytic pyrolysis of individual feedstocks under the same operating conditions. Furthermore, the product distribution of catalytic copyrolysis by varying the mass ratio of ULO/UCO is illustrated in Figure 8, which was investigated with the calculated results based on the catalytic pyrolysis of ULO and UCO individually. The difference in the product distribution at several mass molar ratios of ULO blended with UCO also illustrated the synergistic effect, as described in Figure 9.

As shown in Figure 8, the yield of the liquid product tended to increase when the mass ratios of ULO/UCO were 1:0, 0.9:0.1, and 0.7:0.3, with liquid fractions of 57.58, 60.37, and 63.71 wt %, respectively. The highest liquid yield (66.00 wt %) was obtained when the ULO/UCO mass ratio was 0.5:0.5 and slightly decreased to 65.74 and 61.24 wt % when the ULO/UCO mass ratios were 0.4:0.6 and 0.2:0.8, respectively, while the yield of pyrolysis oil decreased to 61.24 wt % when the catalytic pyrolysis of UCO alone was employed. Notably, the influence of temperature mainly affected the catalytic activity of the ULO alone, causing the randomized degradation of large hydrocarbon chains into free radicals and hydrocarbon radicals. After that, the interaction of free radicals also promoted H-transfer, resulting in accelerated scission of the C−C and C−H bonds to form smaller hydrocarbon compounds, but these are still large hydrocarbon compounds, resulting in difficulty in converting into pyrolysis volatiles properly and resulting in the inability of large volatile vapors to pass through and react with the active site over the catalyst.

While the remarkable thermal gradation, dehydrogenation, and hydrogenation of UCO promoted the conversion of long-chain hydrocarbons from the cofeedstocks into small volatiles, the influence of the acidic catalytic sites on the large surface structure of the Ni/AC catalyst surface also correspondingly increased when the small condensable volatile vapors passed through the porous structure, resulting in enhanced β-scission of the middle hydrocarbon chain into small condensable volatile vapors and selectivity toward hydrocarbons. Therefore, the catalytic copyrolysis of ULO/UCO was strongly influenced by the operating temperature, resulting in the randomized degradation of large hydrocarbon chains to H-radical and hydrocarbon radicals, which also plays a crucial role in the cleavage of C−C bonds and C−H bonds, depolymerization, rearrangement and formation of both cofeedstocks into middle-chain hydrocarbon compounds, and reduction of the thermal stability of the ULO, which accelerated the thermal decomposition of the ULO into medium-sized hydrocarbon chains.[9,15,17] The catalytic activity of the Ni/AC catalyst promoted β-scission and hydrogen transfer, resulting in the formation of straight hydrocarbon chains that properly and continually cracked due to the strong acidic active sites and the pore structure of the Ni/AC catalyst. Therefore, the influence of the mass ratio of ULO/UCO in catalytic copyrolysis clearly increased the yield of naphtha-like from 9.63 to 25.24 wt % when the mass ratio of ULO/UCO was varied from 0.9:0.1 to 0.2:0.8. Notably, the yield of naphtha decreased to 19.02 wt % when UCO was individually employed. This result can be attributed to the fact that most of the UCO was pyrolyzed mainly by thermal decomposition and deoxygenation reactions into small straight hydrocarbon compounds and further cracked at the acidic active site of Ni/AC until the middle hydrocarbon compounds were obtained in the long residue fraction (C_{19}+ hydrocarbon), which is influenced by temperature and the catalyst for further cracking within the pyrolysis reactor, resulting in its conversion to light alkanes with a C_{12} to C_{18} range that consists of the diesel-like fraction (22.82 wt %) and kerosene-like fraction (10.95 wt %), whereas the naphtha-like fraction slightly decreased to 19.02 wt %.

Additionally, the carbonaceous yield decreased monotonically to 10.23, 8.88, 6.16, and 3.01 when the mass ratios of ULO/UCO were 1:0, 0.9:0.1, 0.7:0.3, and 0.5:0.5, respectively. In contrast, carbonaceous formation exhibited the opposite trend, increasing to 3.04, 3.69, and 4.35 wt % when the mass ratios of ULO/UCLO were 0.4:0.6, 0.2:0.8, and 0:1:0.9, respectively. Furthermore, a slight change in the noncondensable gas yield was observed when different ULO/UCO mass ratios were used. This finding indicated that the yield of carbonaceous material consistently increased as the mass of the ULO decreased, which is consistent with the effect of the thermal cracking of UCO alone, with deoxygenation reactions through decarboxylation and decarbonylation to form hydrogen radicals and hydrocarbon radicals that can be further converted into straight hydrocarbons.[9] Subsequently, the secondary cracking reaction of light volatile vapors on the catalyst surface was inhibited by pore blockage, leading to gradual depolymerization and polymerization into the formation of carbonaceous materials and increased deposition at the active site on the surface area of the catalyst, ultimately causing catalyst deactivation.[31]

3.4. Synergistic Study. The individual catalytic pyrolysis of ULO and UCO resulted in differences in thermal decomposition and catalysis according to the chemical composition. ULO is a large-chain hydrocarbon that contains carboxyl and carboxyl groups. Characterization of the ULO revealed that the ULO consists of C−C, C═C, and C═O and a carboxylic group, whereas elemental analysis of the raw ULO revealed H/C mass molar ratios and O/C ratios of 1.81 and 0.17, respectively. The result of the catalytic pyrolysis of UCO alone could be that the fatty acid in UCO was deoxygenated through decarboxylation and decarbonylation reactions, after which thermal degradation enhanced the production of both hydrogen radicals and hydrocarbon radicals. The characterization of the ULO mainly consisted of carbon (82.07 wt %) and hydrogen (15.11 wt %), with a trace of oxygen at 2.82 wt %; the analysis of the mass molar ratio of H/C and O/C ratios of 2.21 and 0.03 revealed that the ULO has greater thermal stability than the UCO. The influence of different proportions of ULO/UCO in catalytic copyrolysis could be attributed to the mechanism of copyrolysis, which generally acknowledges that a free radical reaction from the thermal degradation of a large hydrocarbon compound produces free-radical and chain reactions involved in the copyrolysis of large hydrocarbon compounds and other hydrocarbon compounds. Moreover, raw materials with a high H/C ratio were introduced into the pyrolysis of individual hydrocarbons with a lower H/C ratio to improve the thermal cracking process,[14,18,30] resulting in a

https://doi.org/10.1021/acsomega.4c08111
ACS Omega 2025, 10, 14699−14722

Table 7. Differences in the Actual and Theoretical Product Distributions

	carbonaceous		liquid		naphtha-like		kerosene-like		diesel-like		long residue		gas	
ULO/UCO ratio	actual	theor	actual	theor	actual	theor	actual	theor	actual	theor	actual	theor	actual	theor
1:0	10.23		57.58		8.17		7.46		13.66		28.29		32.19	
0.9:0.1	8.88	9.64	60.37	57.95	9.63	9.26	8.73	7.75	18.87	14.58	23.14	26.37	30.75	32.41
0.7:0.3	6.16	8.47	63.71	58.68	14.42	11.43	7.62	8.33	20.65	16.41	21.02	22.52	30.13	32.86
0.5:0.5	3.01	7.29	66.00	59.41	25.34	13.60	9.83	8.91	13.22	18.24	17.61	18.67	30.99	33.30
0.4:0.6	3.04	6.70	65.74	59.78	25.14	14.68	9.57	9.19	15.35	19.16	15.68	16.75	31.22	33.52
0.2:0.8	3.69	5.53	63.92	60.51	25.24	16.85	8.84	9.77	18.82	20.99	11.02	12.90	32.39	33.97
0:1	4.35		61.24		19.02		10.35		22.82		9.05		34.41	

higher yield, which may be difficult to elucidate in terms of the mechanism of pyrolysis. Therefore, a free radical was the most crucial mechanism to promote or inhibit product distribution from copyrolysis of ULO/UCO.

To understand the synergy of the ULO/UCO in catalytic copyrolysis, the mass ratio of ULO/UCO was varied under the following conditions: 425 °C, inert N_2 flow rate of 50 mL/min, and 5 wt % Ni doped on the AC catalyst by keeping constant 5 wt % of catalyst loading into the feedstock. The yield and product distribution from the experimental copyrolysis with the yield and product distribution were calculated on the basis of the pyrolysis of the ULO and UCO individually. The product distributions from the actual experimental and theoretical calculations are presented in Table 7, and the % difference between the actual experimental and theoretical calculations is illustrated in Figure 9, which is used to describe the synergistic effect of catalytic copyrolysis.

As shown in Figure 9A, only the liquid yield has positive synergistic effects of 4.18, 8.58, and 11.09% when the mass ratios of ULO/UCO are 0.1:0.9 to 0.3:0.7 and 0.5:0.5, respectively. Although the mass ratio of ULO/UCO increased the mass ratio of the blended UCO to ULO from 0.6:0.4 to 0.8:0.2, the percentage differences in the liquid yield decreased only slightly to 9.98 and 5.64%, respectively. This result indicates that the synergistic effect could be attributed to the fact that temperature is an important parameter affecting the thermal degradation of UCO, which has lower thermal stability, and as the pyrolysis temperature increases, UCO is reduced to fatty acids through thermal cracking and deoxygenation through decarbonylation and decarboxylation reactions. Then, a free radical reaction from the thermal degradation of the large hydrocarbon compound produced the free-radical and chain reactions involved in the copyrolysis of both UCO and ULO to form medium hydrocarbon radicals, and the H-donor transfer accelerated the cleavage of the C−H and C−C bonds to smaller values before the catalytic activity was influenced by the β-scission of the middle hydrocarbon chain into small condensable volatiles and further cleavage reactions into small hydrocarbon compounds. The positive effect was represented by increasing the mass ratio of blend UCO to ULO. Notably, UCO plays a crucial role in thermal degradation more easily than does ULO and is more easily decomposed to form free radicals, which play important roles in the cleavage of C−H bonds and C−C bonds. In addition, a hydrocarbon radical also contributes to the cleavage of C−H and C−C bonds in the ULO, resulting in a decrease in the thermal stability of the ULO and promoting the thermal degradation of both the ULO and UCO in copyrolysis reactions to form light hydrocarbons before reacting with the strong acidic active site of the Ni/AC catalyst to properly formulate further product distributions.

The mass ratio of 0.5:0.5 ULO/UCO presented the strongest positive synergistic effect, which can be explained by the increased proportion of mass ratio of UCO playing an important role in the increase in mass/heat transfer, resulting in an increase in the thermal conductivity of ULO and a reduction in the thermal resistance. The hydrogen radical and hydrocarbon radical in ULO have different bond cleavage energies, which may increase the energy of the chemical bond cleavage in ULO/UCO hydrocarbons. Although the mass ratios of ULO/UCO at 0.4:0.6 and 0.2:0.8 also exhibited a positive synergistic effect, there was an increase in the mass ratio of UCO to ULO, which also explains why the thermal degradation of UCO had a strong influence on the copyrolysis reaction, especially on radical fragmentation, and promoted the cleavage of C−C bonds and C−H bonds and H−transfer to smaller hydrocarbon radicals, resulting in the cracking of large hydrocarbon chains into smaller compounds, increasing the heat/mass transfer and reducing the thermal stability of ULO with a higher mass ratio of UCO. The liquid yield was obtained from 0.4:0.6 and 0.2:0.8 mass molar ratios of ULO/UCO, possibly because the slight difference in the synergistic effect may be due to the role of UCO blended in the catalytic copyrolysis reaction.

Additionally, the actual noncondensable gas yields slightly increased from 30.75 to 32.39 wt % when the ULO/UCO mass ratios changed from 0.9:0.1 to 0.2:0.8. The theoretical noncondensable gas yields also tended to increase, but the difference in the actual theoretical noncondensable gas yields with respect to the noncondensable gas yield had a negative synergistic effect. The thermal degradation of UCO plays a critical role in promoting the conversion of long-chain hydrocarbons from cofeedstocks into small volatile compounds.[9,15,17] Consequently, the influence on the catalytic activity was also correspondingly increased when the small condensable volatile vapors passed through the porous structure into the formulation of a small condensable volatile vapor and subsequently cracked into a noncondensable gas due to the influence of high temperature and the secondary cracking of the volatile vapor. As the UCO to ULO mass ratio increased, the thermal degradation of UCO, which has low thermal stability and therefore readily decomposes through deoxygenation and the formation of hydrogen and hydrocarbon radicals, became more prominent than the thermal degradation of ULO in copyrolysis. Therefore, the occurrence of noncondensable gas reveals the ability to thermally decompose UCO and further decompose hydrocarbon radicals into small condensable volatiles, which are further broken down into a large amount of noncondensable gas. These results could be attributed to the fact that the catalytic copyrolysis of ULO/UCO was strongly influenced by the operating temperature, resulting in the randomized degrada-

https://doi.org/10.1021/acsomega.4c08111
ACS Omega 2025, 10, 14699−14722

Table 8. GC/MS Characterization of Pyrolysis Oil

	noncatalyst		AC catalyst			5%Ni/AC	10% Ni/AC		
RT (min)	ULO	UCO	ULO	UCO	ULO/UCO	ULO/UCO	ULO/UCO	chemical compounds	chemical formula
1.288							0.10	pentane	C_5H_{12}
1.423						0.22		hexane	C_6H_{14}
1.784					0.24	0.89	1.19	heptane	C_7H_{16}
2.105			0.11					2,4-dimethylhexane	C_8H_{18}
2.362					1.37	1.88	2.08	octane	C_8H_{18}
3.112					1.44	2.46	3.51	nonane	C_9H_{20}
3.437			0.09					2,3,4-trimethyl-hexane	C_9H_{20}
3.603			0.13					2,4-dimethylheptane	C_9H_{20}
3.848				1.23		2.11		*n*-decane	$C_{10}H_{22}$
3.850					2.53		1.92	decane	$C_{10}H_{22}$
3.897		3.99						decane	$C_{10}H_{22}$
3.970				0.99		0.45		decane	$C_{10}H_{22}$
4.320						1.11	0.40	1,3-dimethylbenzene	C_8H_{10}
4.586					2.25	2.02	1.46	2-ethyl-1,3-dimethylbenzene	$C_{10}H_{14}$
4.608						3.17	3.52	2-ethyl-1,4-dimethylbenzene	$C_{10}H_{14}$
4.613		1.62		1.45				1-undecane	$C_{11}H_{24}$
4.634				1.49	2.16	3.98	4.44	undecane	$C_{11}H_{24}$
4.682		3.05		5.54		1.32		undecane	$C_{11}H_{24}$
5.120					2.31	2.22	2.01	benzene	C_6H_6
5.381				2.59	1.03			naphthalene	$C_{10}H_8$
5.389			0.98			1.95		1-dodecene	$C_{12}H_{24}$
5.410			0.22		2.78	2.23	4.45	dodecane	$C_{12}H_{26}$
5.436		3.82		3.68				dodecane	$C_{12}H_{26}$
6.099						3.97		1-tridecane	$C_{13}H_{28}$
6.102			1.03	1.09				tridecane	$C_{13}H_{26}$
6.104	0.34				3.55		7.24	tridecane	$C_{13}H_{28}$
6.156		4.11		0.65				tridecane	$C_{13}H_{28}$
6.173			0.48			0.48		1,3-tetradecadiene	$C_{14}H_{26}$
6.182				2.01				1-methyl naphthalene	$C_{11}H_{10}$
6.309				1.88				2-methylnaphthalene	$C_{11}H_{10}$
6.773			0.25	1.89		0.65	0.92	tetradecane	$C_{14}H_{30}$
6.780	0.11				3.41	3.24	3.29	tetradecane	$C_{14}H_{30}$
6.828		3.97		1.11				tetradecane	$C_{14}H_{30}$
7.409				2.03		3.91		1-pentadecene	$C_{15}H_{30}$
7.412	1.15			2.28				pentadecane	$C_{15}H_{32}$
7.422			0.24		7.74		4.55	pentadecane	$C_{15}H_{32}$
7.483		8.03		1.93				pentadecane	$C_{15}H_{32}$
8.025			1.63		1.69	3.79	3.67	hexadecane	$C_{16}H_{34}$
8.072		2.45		1.86				hexadecane	$C_{16}H_{34}$
8.536					0.87			1.2-dibutylcyclopentane	$C_{13}H_{26}$
8.595	0.11					0.42		1-heptadecene	$C_{17}H_{34}$
8.611	0.13							3-heptadecene	$C_{17}H_{34}$
8.649		2.67		1.85				heptadecane	$C_{17}H_{36}$
8.890								diethyl phthalate	$C_{12}H_{14}O_4$
8.927			1.21		2.57	0.67	1.29	heptadecane	$C_{17}H_{36}$
9.412			1.36		1.09	0.19	0.23	octadecane	$C_{18}H_{38}$
9.569	1.32							1-nonadecene	$C_{19}H_{38}$
9.668			2.41		0.72	0.38	0.13	nonadecane	$C_{19}H_{40}$
9.703					3.24			2-heptadecanone	$C_{17}H_{34}O$
9.736		0.19		4.03				2-heptadecanone	$C_{17}H_{34}O$
10.103			5.62					*n*-hexadecenoic acid	$C_{16}H_{32}O_2$
10.158			2.52		0.73	1.25	0.08	eicosane	$C_{20}H_{42}$
10.325			4.32					eicosane	$C_{20}H_{42}$
10.377	2.23		2.23					hexadecanoic acid, methyl ester	$C_{17}H_{34}O_2$
10.535			1.82					eicosane	$C_{20}H_{42}$
10.613			4.93			0.31	0.29	heneicosane	$C_{21}H_{44}$
12.477			1.11		1.66	0.43		tetracosane	$C_{24}H_{48}$
12.485	1.36		0.92					2,4-dimethyleicosane	$C_{22}H_{46}$
12.854	5.44		2.87		1.30	0.88		tricosane	$C_{23}H_{48}$

https://doi.org/10.1021/acsomega.4c08111
ACS Omega 2025, 10, 14699−14722

Table 8. continued

	noncatalyst		AC catalyst			5%Ni/AC	10% Ni/AC		
RT (min)	ULO	UCO	ULO	UCO	ULO/UCO	ULO/UCO	ULO/UCO	chemical compounds	chemical formula
12.903	1.68							1-tetracosene	$C_{24}H_{50}$
12.947	4.81							1-hexacosene	$C_{18}H_{38}$
12.982	2.02		1.68					2-methylhexacosane	$C_{26}H_{52}$
12.990	1.31							3-methylheptadecane	$C_{27}H_{56}$
13.218	4.32		2.63		0.80	0.79	0.34	docosane	$C_{22}H_{46}$
14.061	0.92							2-methyloctadecane	$C_{19}H_{40}$

tion of large hydrocarbon chains to H-radical and hydrocarbon radicals, which also plays a crucial role in the cleavage of C−C bonds and C−H bonds, depolymerization, rearrangement, and formation of both cofeedstocks into middle-chain hydrocarbon compounds, and a decrease in the thermal stability of the ULO, which accelerated the thermal decomposition of the ULO into medium-sized hydrocarbon chains. The catalytic activity of the Ni/AC catalyst promoted β-scission and hydrogen transfer, resulting in the formation of straight hydrocarbon chains that properly cracked continually through the strong acidic active site and within the pore structure of the Ni/AC catalyst.[29,34,35,41]

Therefore, the influence of the mass ratio of ULO/UCO in catalytic copyrolysis clearly increased the yield of naphtha-like fraction from 9.63 to 25.24 wt % when the mass ratio of ULO/UCO was varied from 0.9:0.1 to 0.2:0.8. Notably, the yield of naphtha decreased to 19.02 wt % when UCO was individually employed. This result can be attributed to the fact that most of the UCO was pyrolyzed mainly by thermal decomposition and deoxygenation reactions into small straight hydrocarbon compounds and further cracked at the acidic active site of Ni/AC until the middle hydrocarbon compounds were obtained in the long residue fraction (C_{19}^{+} hydrocarbon), which is influenced by temperature and the catalyst for further cracking within the pyrolysis reactor, resulting in its conversion to light alkanes with a C_{12} to C_{18} range that consists of the diesel-like fraction (22.82 wt %) and kerosene-like fraction (10.95 wt %), whereas the naphtha-like fraction slightly decreased to 19.02 wt %.

Figure 9B compares the experimental product distribution results with the theoretically calculated results relevant to the catalytic copyrolysis of the ULO and UCO, and the naphtha-like compounds presented a positive synergistic effect. The % difference in the product distribution represented the positive synergistic effect when the mass molar ratio of ULO/UCO was increased from 0.9:0.1 to 0.2:0.8, although the ULO/UCO ratio was increased by varying the mass molar ratios of 0.9:0.1, 0.7:0.3, 0.5:0.5, 0.4:0.6, and 0.2:0.8, with positive synergies of 4.05, 26.21, 86.39, 71.25, and 49.79%, respectively.

The strong positive synergistic effect at the ULO/UCO mass molar ratio of 0.5:0.5 could be attributed to the thermal degradation of UCO dominating to promote the deoxygenation reaction though decarbonylation, decarboxylation, and the formation of a free radical that affects the C−C bond and C−H bond cleavage and accelerates the conversion of long-chain hydrocarbons of the cofeedstocks into small volatile vapors. The UCO also reduced the thermal stability of ULO and promoted the thermal decomposition of ULO into small hydrocarbon chains. Consequently, an increase in the ULO/UCO mass molar ratio also enhances the promotion of the thermal decomposition of large hydrocarbon chains into free radicals. Therefore, an increase in the ULO/UCO mass molar ratio also promotes the thermal decomposition of large hydrocarbon chains into free radicals and increases the proportion of hydrocarbon radicals that can undergo thermal degradation to form straight hydrocarbon chains. H-radicals and hydrocarbon radicals facilitated the continuous breakdown of C−C bonds and C−H bonds, both of which contribute to the degradation of hydrocarbons to small condensable volatile chains. The acidic active site of Ni doped over the AC catalyst and textural properties such as pore-selective property[29] and the hydrogen transfer through β-scission and carbocation resulted in the formulation the small condensable volatile vapors, and the temperature predominantly introduced secondary cracking to obtain lower carbon atoms ranging from C_5 to C_{12} and increased the percentage of the naphtha-like fraction.[33,40]

Notably, increasing the ratio of blended UCO to ULO/UCO cofeedstock by increasing the mass molar ratio from 0.4:0.6 to 0.2:0.8 also resulted in a positive synergistic effect, but the difference in the percentage of naphtha yield tended to decrease from 71.25 to 49.79%. This is enough to explain the trend of the positive synergistic effect on product distribution in the naphtha-like fraction when a higher proportion of UCO is used in the ULO/UCO feedstocks, which would promote the role of thermal decomposition of both UCO and ULO. Moreover, the radicals generated from UCO also reduce the thermal stability of ULO, resulting in effective thermal degradation to form hydrocarbon chains and further cracking due to the catalytic activity of the Ni/AC catalyst. When the proportion of UCO is too large, the role of UCO becomes too prominent for thermal decomposition since the deoxygenated reaction occurs through carbonylation and carboxylation to form a free radical; then, large hydrocarbon chains also randomly break down into middle hydrocarbon radicals, which are affected by bond cleavage and hydrogen transfer. Generally, the middle hydrocarbon chain reacts with the acidic active site, enhancing the β-scission of C−C bonds and the pore selectivity on Ni/AC catalysts with large surface areas. This process allows the moderately condensable volatile vapors to react with the strong acidic active sites, leading to the formulation of liquid products in the C_5−C_{19} range. The role of the highly acidic catalyst on the mesoporous surface with a large surface area of the support template facilitates the passage of small condensable volatile vapors. This accelerates catalytic cracking within the mesopores for an extended period, enabling the diesel-like fraction (C_{15}−C_{19}) to undergo conversion and further cracking into the naphtha-like fraction (C_5−C_{11}) by the catalytic cracking of UCO individually. This phenomenon suggests that copyrolysis with a relatively high UCO mass ratio does not significantly affect the conversion of ULO/UCO cofeedstocks into the naphtha-like fraction.

However, the synergistic effect of the mass molar ratio of ULO/UCO in catalytic copyrolysis to obtain the other product

https://doi.org/10.1021/acsomega.4c08111
ACS Omega 2025, 10, 14699−14722

distribution has difficulty explaining the positive effect (promotor) or the negative effect (inhibitor) of the ULO/UCO ratio. This result is consistent with the variation in the mass molar ratio of ULO/UCO cofeedstocks, which enhances the conversion of long hydrocarbon chains into a liquid, carbonaceous, or noncondensable gas. Therefore, kinetic and thermodynamic analyses of the mass molar ratio of ULO/UCO involved in catalytic copyrolysis will be conducted in future studies.

3.5. Characterization of Liquid Fuel Properties. *3.5.1. Analyses of Chemical Compounds via GC/MS.* The chemical compounds produced from pyrolysis and catalytic copyrolysis at 425 °C, an inert N_2 flow rate of 50 mL/min, and 5 wt % Ni doped with 5 wt % catalyst loaded into the feedstocks were analyzed via GC/MS, and the percentage of the relative peak area that matched the NIST chemical data is shown in Table 8. Analysis of the pyrolysis oil revealed that the peak intensity from the retention time (RT) ranged from 1.288 to 13.218 min, whereas the peak intensities of both the ULO and UCO raw materials ranged from 8.025 to 17.055 min and 10.103 to 40.959 min, respectively. This is likely due to the existence of large hydrocarbon chains, C═C bonds, C═O bonds, and −COOH groups, which identify the species of raw material because it is composed of large amounts of oxygen and moisture when the GC/MS technique is employed. In fact, in this study, the % peak area was not proportional to the amount of chemical compounds.

As shown in Table 8, the pyrolysis of individual ULO without the catalyst presented significantly intense peak areas at RT values of 7.412, 12.854, and 13.218 min, which are relevant to the chemical compounds of straight aliphatic hydrocarbon compounds ($C_{15}H_{32}$, $C_{19}H_{40}$, and $C_{22}H_{46}$); the RT values of 12.485, 12.982, and 12.990 min presented branch aliphatic hydrocarbons ($C_{22}H_{46}$, $C_{26}H_{52}$, and $C_{27}H_{56}$), whereas the RTs of 12.903 and 12.947 min represented the olefinic hydrocarbon compounds of $C_{24}H_{50}$ and $C_{18}H_{38}$, respectively, which is also consistent with the production distributions in the diesel-like fraction and the long residue fraction. The analysis revealed that the ULO is a large hydrocarbon chain with a carbon number of up to 55 carbon atoms that has undergone depolymerization and oxidation with air/oxygen during use. When the ULO without a catalyst was pyrolyzed, the conversion of the ULO was affected mainly by the influence of temperature, which also accelerated the randomized degradation of large hydrocarbon chains through the free radical mechanism to form large formulations of shortened radicals. The radical causes further degradation of the hydrocarbon chains until the carbon atoms are reduced into small volatile vapors and continually crack via a secondary reaction, resulting in the formation of a large amount of noncondensable gases.

The large hydrocarbon chain in UCO was cracked into shortened hydrocarbons by the influence of high temperature, resulting in a randomized thermal degradation mechanism in which the deoxygenation of ULO was reduced to fatty acids through decarbonylation and decarboxylation reactions. The influence of temperature also influences mainly the cleavage of the C−C and C−H bonds of medium hydrocarbon chains into hydrogen and hydrocarbon radicals through the radical mechanism, causing large hydrocarbon chains to break down into medium hydrocarbon chains; some of them are therefore continually broken down into small volatile vapors and further undergo secondary cracking into large amounts of noncondensable gas. Moreover, some medium hydrocarbon compounds form large hydrocarbon chains through repolymerization reactions. The GC/MS analyses of UCO pyrolysis oil revealed the occurrence of straight aliphatic hydrocarbon compounds from $C_{10}C_{22}$, $C_{11}H_{24}$, $C_{12}H_{26}$, $C_{13}H_{28}$, $C_{14}H_{30}$, $C_{15}H_{32}$, $C_{16}H_{34}$, and $C_{17}H_{36}$ from the RT of 3.89 to 8.649 min, whereas some oxygenated compounds of 2-heptadecanone and methyl ester hexadecenoic acid were also identified at the RT of 9.736 min (0.19% of peak area) and 10.377 min (4.92% of peak area), which correspond to the diesel-like fraction obtained during the pyrolysis of UCO under mild processing conditions.

The pyrolysis of individual ULO and UCO via AC catalysts resulted in small hydrocarbon compounds affected by the influence of catalytic activity and porosity with a large surface area, which accelerated the cleavage of C−C bonds and hydrogen transfer to form medium hydrocarbon compounds. The acid activity sites of the AC catalyst promoted β-scission into shortened condensable volatile vapors, whereas the hydrogenation of aliphatic hydrocarbons occurred, resulting in the formation of substituted-aliphatic hydrocarbons, e.g., 2,3,4-trimethyl-hexane, 2,4-dimethyl-heptane, and 2,4-dimethyl-eicosane, which are present in ULO pyrolysis oil. Additionally, the catalytic pyrolysis of the ULO also produced a straight aliphatic hydrocarbon from $C_{12}H_{26}$ to $C_{23}H_{48}$, and slight peak areas of olefin hydrocarbon compounds were identified for 1-dodecene (0.98% of the peak area) and tetradeca-1,3-diene (0.48% of the peak area). The UCO catalyst also has catalytic performance after thermal degradation, which also enhances the reduction of a large hydrocarbon chain to remove the carbonyl group and carboxyl group via decarbonylation and decarboxylation and then the formulation of free radicals due to the effect of temperature, resulting in the cleavage of the C−C bond and hydrogen transfer of fatty acids to intermediate hydrocarbon radicals and condensable volatile vapors. After that, both the strength acidity and the porosity of the large surface area of the AC catalyst promote the catalytic cracking of medium hydrocarbon chains through β-scission and hydrogenation reactions to form alkanes of the C_{10}−C_{16} carbon range, which corresponds to the catalytic conversion of the ULO to kerosene-like and diesel-like fractions according to the analysis of product distribution.

GC/MS analysis of the copyrolysis product using the AC catalyst also revealed a peak of straight aliphatic hydrocarbons from C_7H_{16} to $C_{24}H_{50}$, but the main proportion of aliphatic hydrocarbons was obtained in the carbon range of $C_{10}H_{22}$ to $C_{17}H_{36}$, which is consistent with the analysis of the product distribution in which the pyrolysis oil also consists of kerosene-like and diesel-like fractions, whereas 2-heptadecanone was slightly observed in the copyrolysis of UCO because the UCO contained both carbonyl- and carboxyl- groups pyrolyzed under the influence of temperature, but the catalytic activity could not allow the reduction of the oxygenated hydrocarbon compounds within the active site and the mesopores over the AC catalyst.

When the Ni-doped/AC catalyst was employed for the catalytic copyrolysis of ULO/UCO, the GC/MS analysis illustrated a peak of straight aliphatic hydrocarbons in the carbon range from C_7 to C_{12}, which was consistent with the influence of the strength of the acid active site and mesopores. Furthermore, some volatile vapors can pass through and restructure inside the pore selectively: isomerization, cyclization, and hydrogenation; oligomerization of condensable

https://doi.org/10.1021/acsomega.4c08111
ACS Omega 2025, 10, 14699−14722

Table 9. Physicochemical Analyses of Copyrolysis Oil

components	non-catalyst ULO	non-catalyst UCO	AC SLO	AC UCO	non-catalyst ULO/UCO	AC ULO/UCO	5%Ni/AC ULO/UCO	10%Ni/AC ULO/UCO	method of analysis
C	82.03	77.73	74.54	82.18	78.51	83.35	83.81	83.15	ASTM D3176
H	16.78	11.28	13.24	11.61	12.54	15.39	15.76	16.44	
O	1.01	10.99	11.2	6.21	8.95	0.98	0.43	0.41	
N	0.18	n.d.	1.02	n.d.	n.d.	0.28	n.d.	n.d.	
S	n.d.[a]	n.d.	n.d.	n.d.	n.d.	n.d.	n.d.	n.d.	
H/C	2.45	1.74	2.13	1.70	1.92	2.22	2.26	2.37	calculation
O/C	0.01	0.11	0.11	0.06	0.09	0.01	n.a.[b]	n.a.	calculation
HHV (MJ/kg)	51.51	40.42	42.10	43.25	42.85	49.97	50.76	51.51	calculation
HHV (MJ/kg)	43.65	37.56	44.09	39.78	40.68	44.16	44.98	45.73	ASTM D240
kinematic viscosity	51.54	23.26	17.29	16.62	37.84	15.27	14.66	11.57	ASTM D445-19

[a]n.d. = not detectable. [b]n.a. = not acceptable.

volatile vapors to form alkene and aromatic compounds; and 2-ethyl-1,3-demethylbenzene and 2-ethyl-1,4-demethylbenzene, which were observed at the RTs of 4.586 and 4.608 min, respectively. This result reveals that the role of NiO on the AC catalyst enhances the C−C bond cleavage due to the acidic active site on the AC support and that the rate of β-scission formation, which also breaks down the C−C bond through the AC catalyst, is promoted because an increase in the strength of the acidic active site affects the rearrangement of the smaller hydrocarbon chain through the mesopore and large surface structure with a high pore volume to form a straight aliphatic hydrocarbon chain in the range of C_5−C_{19}. The small volatile vapor from the thermal cracking of both ULO/UCO also continually cracked and could be condensable into suitable light hydrocarbon compounds that were established at lower concentrations of Ni doped with the AC catalyst, whereas the strength of the acidic active sites of AC, which tended to increase with the modification of Ni to the AC catalyst, resulting in a decrease in the medium-strength hydrocarbon chains, was shortened by the β-scission of C−C bonds, and the secondary cracking of volatile vapor also formed into small-molecule volatiles to increase the liquid yield, which was mostly in the naphtha-like fraction.

3.5.2. Physicochemical Analyses. Table 9 shows the results of the analyses of the physicochemical properties of the copyrolysis oil. The H/C and O/C mass molar ratios decreased from the thermal cracking of the ULO to 2.49 and 0.02, respectively. However, the pyrolysis oil from UCO showed a significant decrease in the O/C mass molar ratio to 0.11, resulting in the HHV of pyrolysis of UCO increasing to 37.56 MJ/kg compared with that of the raw UCO (36.01 MJ/kg).

Notably, the deoxygenated reaction reduced UCO to fatty acids and hydrocarbon radicals through decarbonylation and decarboxylation reactions, and the formation of CO and CO_2 in noncondensable gas was observed. Furthermore, the deoxygenation of UCO during pyrolysis without the catalyst improved the higher heating value in the pyrolysis oil, which was related to the decrease in the oxygen content through decarbonylation and decarboxylation and the slight increase in the HHV in the pyrolysis oil of the ULO. The pyrolysis oil from the ULO alone represented a gradual decrease in the oxygen content to 0.14%, which was caused by thermal cracking at high temperatures to remove residual moisture from the raw ULO, resulting in a slight increase in the HHV to 44.09 MJ/kg, whereas the kinematic viscosity of the pyrolysis oil decreased only slightly with increasing temperature, which accelerated the randomized cleavage of large chains in the ULO into hydrogen and hydrocarbon radicals. The hydrocarbon chains that are shortened from the radical can undergo further cleavage of C−C and C−H bonds to form medium and small hydrocarbons, which are continually broken down into condensable volatiles from secondary reactions, but some of the hydrocarbon chains may also undergo depolymerization and repolymerization, returning to the formulation of large hydrocarbon chains. Moreover, pyrolysis of the ULO and UCO produced pyrolysis oil that had a significant decrease in kinematic viscosity to 51.54 and 23.26 mm^2/s, respectively, compared with the raw ULO (106.49 mm^2/s) and raw UCO (96.81 mm^2/s).

The influence of the AC catalyst was investigated, and the middle hydrocarbon chain and condensable volatile vapor were initiated by the influence of the temperature and then catalyzed by the catalyst. Elemental analysis and analysis of the physicochemical properties of the catalytic pyrolysis of individual ULO and UCO when AC was employed revealed the catalytic activity of the AC catalyst at both the acidic active site and the pore selectivity, which accelerated the β-scission of C−C bonds into small hydrocarbon chains. Then, the mesoporous and large surface areas of AC also facilitated the hydrogen transfer reaction that took place at the active site, further hydrogenation, isomerization, and oligomerization to obtain C_5−C_{19} pyrolysis oil. This observation was consistent with the analysis of the product distribution, and elemental analyses revealed an increase in the H/C mass molar ratio. The amount of oxygen decreased with increasing UCO, resulting in the HHV obtained from the ULO and UCO pyrolysis oils increasing to 44.09 and 39.78 MJ/kg, respectively, and the kinematic viscosity decreased to 17.29 and 16.62 mm^2/s, respectively, because the influence of thermal decomposition and catalytic cracking promoted the cleavage of C−C and C−H bonds into smaller chains that could react in the mesopores of the AC catalysts.

The comparison of the elemental analysis and physicochemical results of the copyrolysis of the ULO/UCO catalyst and the catalytic copyrolysis using the AC catalyst revealed the role of ULO/ULO in copyrolysis, revealing that the influence of temperature increased the degree of deoxygenation and thermal degradation of UCO, which can undergo decarbonylation and decarboxylation and form a hydrocarbon radical that can promote the bond cleavage of large hydrocarbon chains in both the UCO and the ULO. In addition, the

https://doi.org/10.1021/acsomega.4c08111
ACS Omega 2025, 10, 14699−14722

increase in hydrocarbon radical content reduces the thermal stability of the ULO, resulting in a shortened hydrocarbon chain. The copyrolysis oil had an oxygen content of approximately 8.95 wt % when ULO/UCO was pyrolyzed without a catalyst and 0.98 wt % when an AC catalyst was used, suggesting that the AC catalyst has acidic active sites and that the textural properties of the catalyst enhance the contact of small condensable volatiles with the catalyst and promote deoxygenation, H-transfer, and β-scission facilitating the cleavage of C−C bonds, hydrogenation, and isomerization, resulting in a short hydrocarbon chain in the carbon range of C_5−C_{19}, corresponding to the product distribution analysis, which revealed the conversion of long-chain hydrocarbons to shortened aliphatic hydrocarbons composed of diesel-like (8.44 wt %), kerosene-like (12.11 wt %), and naphtha-like (18.93 wt %) when the AC catalyst was employed. Therefore, the HHV of the catalytic copyrolysis of ULO/UCO significantly increased to 44.16 MJ/kg compared with that of the copyrolysis of ULO/UCO without the catalyst (40.68 MJ/kg), and the kinematic viscosity also tended to decrease from 37.84 to 5.27 mm^2/s when AC was employed. The comparison of the catalytic copyrolysis of ULO/UCO using the difference between the Ni-doped and AC catalysts demonstrated the catalytic performance of the acid active site in terms of its ability to catalyze the conversion of the long C_{19}^+ hydrocarbon chain into a shortened, condensable volatile vapor, which was achieved by β-scission and C−C bond cleavage that occurred on the large active site of the AC catalyst. Then, hydrogenation, isomerization, and oligomerization increased its conversion to the formulation of straight aliphatic hydrocarbon compounds, mainly in the naphtha-like (C_5−C_{12}) range. The strong acidic active site from the Ni doped on the AC catalyst may have resulted in the HHV of copyrolysis oil from ULO/UCO (44.98 to 45.73 MJ/kg) and a lower kinematic viscosity (4.66 to 4.57 mm^2/s) when the amount of Ni doped from 5 and 10 wt % to the AC catalyst increased, which corresponds to the occurrence of product distribution in the naphtha-like fraction.

3.6. Chemical Reaction Pathways of Copyrolysis. As seen from the series of experimental designs for catalytic copyrolysis, the influence of temperature is an important operating condition of thermal decomposition reactions. Both carbonylation and decarboxylation of fatty acids in UCO affect the thermal degradation of UCO through a deoxygenation reaction. Then, the thermal degradation of large hydrocarbon chains into radicals, H-radicals, and hydrocarbon radicals occurs and continues to affect the breakdown of the C−C bonds and C−H bonds of large to middle hydrocarbon chains. Although the blending of the ULO results in greater thermal stability than that of the UCO, the high H/C ratio feedstock is introduced into the pyrolysis of individual hydrocarbons with a lower H/C ratio, including a low caloric value, to improve the thermal cracking process. The ULO reduces the thermal stability, which is relevant to the thermal degradation of large hydrocarbon compounds, and the primary reactions take place through free radicals and the cleavage of C−H and C−C bonds into the middle hydrocarbon chain. The operating temperature of 450 °C increases the thermal decomposition of both the ULO and UCO into smaller hydrocarbon radicals that form middle hydrocarbon compounds. Consequently, the role of the catalyst enhances the acceleration of C−C and C−H scission to break down and the formation of straight hydrocarbon chains. While the higher hydrogen-donating capacity of UCO decreases the thermal stability of the ULO, which increases the thermal degradation of C−C bonds and C−H bonds, Ni doped into the AC catalyst, which is relevant to the acid activity, is mainly responsible for β-scission and H-transfer, resulting in the C−C scission of hydrocarbon chains to condensable volatile vapors. The role of the acidic active site over the textural structure of activated carbon, including the composition of the ULO with more hydrogen and a limited content of oxygen, affects cracking by C−H bond scission, leading to thermal decomposition, β-scission, and H-transfer of long hydrocarbon chains, which are cleaved into small hydrocarbon chains, enhancing the hydrogenation reaction and cracking into a condensable volatile vapor that forms into a linear short hydrocarbon compound. The porosity with a large surface structure and its pore-selective properties also enable successive isomerization and hydrogenation to account for the straight aliphatic hydrocarbon compounds and promote the formation of proper hydrocarbon vapors that can condense to achieve alkanes with carbon ranging from C_5 to C_{12} hydrocarbon compounds and various chemical compounds with carbon ranging from C_{12} to C_{19}.

When the catalyst loading was increased to 20% loading to the cofeedstock weight, the rate of catalytic copyrolysis of ULO/UCO was directly proportional to the number of active sites on the catalyst; thus, the increase in catalyst loading increased the number of acidic active sites, which accelerated hydrocarbon bond cleavage for the catalytic cracking of ULO/UCO into condensable volatile compounds at the carbon ranging from C_5 to C_{19}, whereas excessive catalyst loading increased the number of active sites, which promoted the catalytic activity into shorter hydrocarbon compounds, and some further cracking continued because the long residence time and high operating temperature enhanced the secondary cracking reaction, affecting the conversion of small volatile vapors into condensable volatile compounds and the formation of noncondensable gases.

Moreover, some of the small hydrocarbon chains enhance the depolymerization reaction into larger hydrocarbon chains when catalytic copyrolysis occurs at high temperatures and long residence times, resulting in deactivation of the catalyst due to the formation of coke at the acid active site of the catalyst, including obscuration of the active site or blockage within the mesopore.

4. CONCLUSIONS

The catalytic copyrolysis of ULO with UCO over the Ni modification of the activated carbon catalyst was investigated for the production of naphtha-like fuels and chemicals. The temperature has the greatest influence on promoting the deoxygenation of UCO through several deoxygenation reactions and thermal degradation into a radical, which continues to affect the breakdown of the C−C bonds to the middle hydrocarbon chain, whereas the ULO reduces the thermal stability, which is relevant to thermal degradation, and the primary reactions take place through the free radical into the middle hydrocarbon chain. The 5 wt % Ni doped on the AC catalyst is related to the strength of the acid activity, which is mainly responsible for C−C scission and H-transfer, resulting in the formation of condensable volatile vapors, whereas the porosity, which has a large surface structure and pore-selective properties, also promotes the formation of hydrocarbon vapors that can condense into C_5−C_{12} compounds and various chemical compounds in the carbon range

https://doi.org/10.1021/acsomega.4c08111
ACS Omega 2025, 10, 14699−14722

of C_{12}−C_{19}. However, excessive catalyst loading increased the number of active sites, which promoted catalytic activity into shorter hydrocarbon compounds and further secondary cracking, affecting the formation of noncondensable gas. The optimal condition for catalytic copyrolysis of ULO/UCO presented the highest yield of naphtha-like fraction (25.34 wt %), which was obtained when the temperature was 425 °C, the N_2 carrier flow rate was 50 mL/min, the ULO/UCO ratio was 0.5:0.5, 5 wt % Ni was modified into the AC catalyst, and 5 wt % of Ni/AC catalyst loading into the feedstock was used. The synergy of ULO/UCO under catalytic copyrolysis conditions illustrated that the trend of the actual liquid yield was greater than the theoretical value when the ULO/UCO ratio was varied from 0.9:0.1 to 0.5:0.5 and also illustrated a positive effect when the ULO/UCO ratio was varied from 0.5:0.5 to 0.1:0.9, while the actual naphtha-like fraction had the greatest difference (86.39%) from the theoretical value, which indicated the positive effect of the ULO/UCO ratio of 0.5:0.5. Furthermore, the catalytic copyrolysis of ULO/UCO using Ni doped into the AC catalyst was more favorable for improving the straight aliphatic hydrocarbons in the naphtha-like C_5−C_{12} range and valuable C_{12}−C_{19} compounds. However, the findings of this study highlight the influence of the optimal operating parameters through a systematic experimental design and illustrated the synergistic approach to determine the benefits of using different ULO/UCO mass molar ratios; the significant parameters of the copyrolysis of ULO/UCO may have an interaction that enhanced to promote the conversion of ULO/UCO through catalytic pyrolysis reaction to produce sustainable fuels. Although studying the optimal process parameters and synergistic effects provides sufficient insight into the copyrolysis reaction mechanism, further investigations should involve thermodynamic calculations and kinetic studies, which were also used to predict and clarify the chemical mechanisms and pathways of the pyrolysis more precisely.

AUTHOR INFORMATION

Corresponding Author

Witchakorn Charusiri − *Department of Environment, Faculty of Environmental Culture and Ecotourism, Srinakharinwirot University, Bangkok 10110, Thailand;* orcid.org/0000-0002-4058-0367; Email: witchakorn@swu.ac.th

Authors

Naphat Phowan − *Department of Environment, Faculty of Environmental Culture and Ecotourism, Srinakharinwirot University, Bangkok 10110, Thailand*

Tharapong Vitidsant − *Department of Chemical Technology, Faculty of Science, Chulalongkorn University, Bangkok 10330, Thailand; Center of Fuels and Energy from Biomass, Chulalongkorn University, Kaengkhoi, Saraburi 18110, Thailand*

Complete contact information is available at: https://pubs.acs.org/10.1021/acsomega.4c08111

Author Contributions

Witchakorn Charusiri: conceptualization, methodology, investigation, visualization, validation, writing—original draft, review and editing, and funding acquisition. Naphat Phowan: investigation and visualization. Tharapong Vitidsant: conceptualization, resources, validation, and writing—review and editing.

Notes

The authors declare no competing financial interest.

ACKNOWLEDGMENTS

This research has received funding from the Srinakharinwirot University Innovative Research Promotion Endowment Fund, allocated by the Strategic Wisdom and Research Institute Srinakharinwirot University (Contract No. 565/2564). In addition, the authors acknowledge the support of the Center of Fuels and Energy from Biomass, Chulalongkorn University, and the Faculty of Environmental Culture and Ecotourism, Srinakharinwirot University, for their assistance in analyzing samples and characterizing of the pyrolysis products.

REFERENCES

(1) Londoño Feria, J. M.; Nausa Galeano, G. A.; Malagón-Romero, D. H. Production of bio-oil from waste cooking oil by pyrolysis. *Chem. Eng. Technol.* **2021**, *44*, 2341−2346.

(2) Hosseinzadeh-Bandbafha, H.; Li, C.; Chen, X.; Peng, W.; Aghbashlo, M.; Lam, S. S.; Tabatabaei, M. Managing the hazardous waste cooking oil by conversion into bioenergy through the application of waste-derived green catalysts: a review. *J. Hazard Mater.* **2022**, *424*, No. 127636.

(3) Khalit, W. N. A. W.; Asikin-Mijan, N.; Marliza, T. S.; Gamal, M. S.; Shamsuddin, M. R.; Saiman, M. I.; Taufiq-Yap, Y. H. Catalytic deoxygenation of waste cooking oil utilizing nickel oxide catalysts over various supports to produce renewable diesel fuel. *Biomass. Bioenerg.* **2021**, *154*, No. 106248.

(4) Balboul, B. A. A.; Abdelrahman, A. A.; Salem, H. M.; Mohamed, E. A.; Osman, D. I.; Rabie, A. M. Enhanced production of liquid fuel via catalytic cracking of used sunflower oil catalyzed by Praseodymium supported alumina. *J. Mol. Liq.* **2022**, *367*, No. 120562.

(5) Pimenta, J. L. C. W.; de Oliveira Camargo, M.; Belo Duarte, R.; dos Santos, O. A. A.; de Matos Jorge, L. M. Deoxygenation of vegetable oils for the production of renewable diesel: improved aerogel based catalysts. *Fuel.* **2021**, *290*, No. 119979.

(6) Li, L.; Ding, Z.; Li, K.; Xu, J.; Liu, F.; Liu, S.; Yu, S.; Xie, C.; Ge, X. Liquid hydrocarbon fuels from catalytic cracking of waste cooking oils using ultrastable zeolite USY as catalyst. *J. Anal. Appl. Pyrol.* **2016**, *117*, 268−272.

(7) Negm, N. A.; Rabie, A. M.; Mohammed, E. A. Molecular interaction of heterogeneous catalyst in catalytic cracking process of vegetable oils: chromatographic and biofuel performance investigation. *Appl. Catal. B: Environ.* **2018**, *239*, 36−45.

(8) Wang, Y.; Cao, Y.; Li, J. Preparation of biofuels with waste cooking oil by fluid catalytic cracking: The effect of catalyst performance on the products. *Renew. Energy.* **2018**, *124*, 34−39.

(9) Patel, N.; Shadangi, K. P. Thermochemical conversion of waste engine oil (WEO) to gasoline-rich crude oil. *J. Mater. Cycles Waste Manage.* **2020**, *22*, 536−546.

(10) Santhoshkumar, A.; Ramanathan, A. Recycling of waste engine oil through pyrolysis process for the production of diesel like fuel and its uses in diesel engine. *Energy.* **2020**, *197*, No. 117240.

(11) Ahmad, I.; Khan, R.; Ishaq, M.; Khan, H.; Ismail, M.; Gul, K.; Ahmad, W. Valorization of spent lubricant engine oil via catalytic pyrolysis: Influence of barium-strontium ferrite on product distribution and composition. *J. Anal. Appl. Pyrol.* **2016**, *122*, 131−141.

(12) Sasidhar, K. B.; Arkin, G.; Gowtham, G.; Somasundaram, M.; Vuppaladadiyam, A. K. Conversion of waste ship-oil sludge into renewable fuel: Assessment of fuel properties and techno-economic viability of supplementing and substituting commercial fuels. *J. Clean. Prod.* **2023**, *427*, No. 139362.

(13) Izaddoust, S.; Hita, I.; Zambrano, N.; Trueba, D.; Palos, R.; Zhang, W.; Epelde, E.; Arandes, J. M.; Castaño, P. Fuel production via catalytic cracking of pre-hydrotreated heavy-fuel oil generated by marine-transport operations. *Fuel.* **2022**, *325*, No. 124765.

(14) Yue, L.; Li, G.; He, G.; Guo, Y.; Xu, L.; Fang, W. Impacts of hydrogen to carbon ratio (H/C) on fundamental properties and supercritical cracking performance of hydrocarbon fuels. *Chem. Eng. J.* **2016**, *283*, 1216−1223.
(15) Kiran, S.; Martin, M. L. J.; Sonthalia, A.; Varuvel, E. G. Synergistic effect of hydrogen and waste lubricating oil on the performance and emissions of a compression ignition engine. *Int. J. Hydrogen Energy* **2023**, *48* (60), 23296−23307.
(16) Wang, J.; Qi, X.; Dong, X.; Zhang, K.; Luo, S. Mechanistic insights into co-pyrolysis of waste tires and waste lubricating oil: Kinetics and thermal behavior study. *Energ Source. Part A* **2023**, *45* (3), 8568−8583.
(17) Huo, E.; Liu, C.; Xin, L.; Zhang, Y.; Zhao, Y.; Qian, M.; Lin, X.; Lei, H. Jet fuel range hydrocarbon production by co-pyrolysis of low density polyethylene and wheat straw over an activated carbon catalyst. *Sustainable Energy Fuel.* **2021**, *5* (23), 6145−6156.
(18) Charusiri, W.; Phowan, N.; Permpoonwiwat, A.; Vitidsant, T. Catalytic copyrolysis of used waste plastic and lubricating oil using Cu-modification of a spent fluid catalytic cracking catalyst for diesel-like fuel production. *ACS Omega.* **2023**, *8* (43), 40785−40800.
(19) Zhang, Y.; Fu, Z.; Wang, W.; Ji, G.; Zhao, M.; Li, A. Kinetics, product evolution, and mechanism for the pyrolysis of typical plastic waste. *ACS Sustain Chem. Eng.* **2022**, *10* (1), 91−103.
(20) Ma, Z.; Hou, X.; Chen, B.; Zhao, L.; Yuan, E.; Cui, T. Experiment and modeling of coke formation and catalyst deactivation in n-heptane catalytic cracking over HZSM-5 zeolites. *Chin J. Chem. Eng.* **2023**, *55*, 165−172.
(21) Li, C.; Ma, J.; Xiao, Z.; Hector, S. B.; Liu, R.; Zuo, S.; Xie, X.; Zhang, A.; Wu, H.; Liu, Q. Catalytic cracking of Swida wilsoniana oil for hydrocarbon biofuel over Cu-modified ZSM-5 zeolite. *Fuel.* **2018**, *218*, 59−66.
(22) Ma, W.; Liu, B.; Zhang, R.; Gu, T.; Ji, X.; Zhong, L.; Chen, G.; Ma, L.; Cheng, Z.; Li, X. Co-upgrading of raw bio-oil with kitchen waste oil through fluid catalytic cracking (FCC). *Appl. Energy.* **2018**, *217*, 233−240.
(23) Mammadova, T.; Abbasov, M.; Movsumov, N.; Latifova, T.; Hasanova, A.; Kocharli, Z.; Khalafova, İ.; Abbasov, V. Production of diesel fractions by catalytic cracking of vacuum gas oil and its mixture with cottonseed oil under the influence of a magnetic field. *Egypt. J. Pet.* **2018**, *27* (4), 1029−1033.
(24) Xiang, L.; Li, H.; Qu, Q.; Lin, F.; Yan, B.; Chen, G. In-situ catalytic pyrolysis of heavy oil residue with steel waste to upgrade product quality. *J. Anal. Appl. Pyrol.* **2022**, *167*, No. 105676.
(25) Zhang, Y.; Duan, D.; Lei, H.; Villota, E.; Ruan, R. Jet fuel production from waste plastics via catalytic pyrolysis with activated carbons. *Applied Energy.* **2019**, *251*, No. 113337.
(26) Negm, N. A.; Betiha, M. H. A.; El-Wakeel, N. M. H.; Mohamed, E. A. An insight into recent developments in sustainable biofuel production using activated carbon catalyst produced via valorization of agricultural biomass: Challenges, and environmental prospective. *Ind. Crops Prod.* **2024**, *209*, No. 117991.
(27) Duan, D.; Zhang, Y.; Wang, Y.; Lei, H.; Wang, Q.; Ruan, R. Production of renewable jet fuel and gasoline range hydrocarbons from catalytic pyrolysis of soapstock over corn cob-derived activated carbons. *Energy.* **2020**, *209*, No. 118454.
(28) Maneechakr, P.; Karnjanakom, S. Improving the bio-oil quality via effective pyrolysis/deoxygenation of palm kernel cake over a metal (Cu, Ni, or Fe)-Doped carbon catalyst. *ACS Omega.* **2021**, *6*, 20006−20014.
(29) Lin, Q.; Zhang, S.; Wang, J.; Yin, H. Synthesis of modified char-supported Ni−Fe catalyst with hierarchical structure for catalytic cracking of biomass tar. *Renew. Energy.* **2021**, *174*, 188−198.
(30) Li, P.; Pan, H.; Wan, K.; Zhou, S.; Zhang, Z.; Hong, D.; Zhang, Y. Jet fuel-range hydrocarbon production from catalytic pyrolysis of low-density polyethylene by metal-loaded activated carbon Sustainable. *Energy Fuel.* **2022**, *6* (9), 2289−2305.
(31) Liu, H.; Ye, C.; Ye, Z.; Zhu, Z.; Wang, Q.; Tang, Y.; Luo, G.; Guo, W.; Dong, C.; Li, G.; Xu, Y.; Wang, Q. Catalytic cracking and catalyst deactivation/regeneration characteristics of Fe-loaded biochar catalysts for tar model compound. *Fuel.* **2023**, *334*, No. 126810.
(32) Rodriguez, Y.; Guerra, R.; Vizuete, K.; Debut, A.; Streitwieser, D. A.; Mora, J. R.; Ponce, S. Kinetic study of the catalytic cracking of waste motor oil using biomass-derived heterogeneous catalysts. *Waste Manage.* **2023**, *167*, 46−54.
(33) Ding, K.; Liu, S.; Huang, Y.; Liu, S.; Zhou, N.; Peng, P.; Wang, Y.; Chen, P.; Ruan, R. Catalytic microwave-assisted pyrolysis of plastic waste over NiO and HY for gasoline-range hydrocarbons production. *Energy Convers. Manag.* **2019**, *196*, 1316−1325.
(34) Amjad, U.; Tajjamal, A.; Ul-Hamid, A.; Faisal, A.; Zaidi, S. A. H.; Sherin, L.; Mir, A.; Mustafa, M.; Ahmad, N.; Hussain, M.; Park, Y.-K. Catalytic cracking of polystyrene pyrolysis oil: Effect of Nb_2O_5 and NiO/Nb_2O_5 catalyst on the liquid product composition. *J. Waste Manag.* **2022**, *141*, 240−250.
(35) Zhang, S.; Yin, H.; Wang, J.; Zhu, S.; Xiong, Y. Catalytic cracking of biomass tar using Ni nanoparticles embedded carbon nanofiber/porous carbon catalysts. *Energy.* **2021**, *216*, No. 119285.
(36) Charusiri, W.; Vitidsant, T. Response Surface Methodology Optimization of Biofuels Produced by Catalytic Pyrolysis of Residual Palm Oil from Empty Fruit Bunch over Magnesium Oxide. *J. Chem. Eng. Jpn.* **2017**, *50* (9), 727−736.
(37) American Oil Chemists' Society AOCS Official Method Ca 2c-25: Moisture and Volatile Matter, Air Oven Method. In *Official Methods and Recommended Practices of the AOCS*, 7th ed.; Firestone, D., Ed.; AOCS Press: Urbana, IL, 2017.
(38) Kasetsupsin, P.; Vitidsant, T.; Permpoonwiwat, A.; Phowan, N.; Charusiri, W. Combined Activated Carbon with Spent Fluid Catalytic Cracking Catalyst and MgO for the Catalytic Conversion of Waste Polyethylene Wax into Diesel-like Hydrocarbon Fuels. *ACS Omega.* **2022**, *7* (23), 20306−20320.
(39) Miao, P.; Zhu, X.; Guo, Y.; Miao, J.; Yu, M.; Li, C. Combined mild hydrocracking and fluid catalytic cracking process for efficient conversion of light cycle oil into high-quality gasoline. *Fuel.* **2021**, *292*, No. 120364.
(40) Yaisamlee, R.; Reubroycharoen, P. Light olefin production from the catalytic cracking of fusel oil in a fixed bed reactor. *Biomass Bioenerg.* **2021**, *153*, No. 106217.
(41) Khalid, M. A.A.; Abdullah, N.; Ibrahim, M. N. M.; Taib, R. M.; Rosid, S. J. M.; Shukri, N. M.; Yahaya, N.; Abdullah, W. N. B. W. Catalytic pyrolysis of waste oil into hydrocarbon fuel utilizing cerium oxide catalyst. *Korean J. Chem. Eng.* **2022**, *39*, 1487−1495.
(42) Zhang, D.; Zong, P.; Wang, J.; Gao, H.; Guo, J.; Wang, J.; Wang, Y.; Tian, Y.; Qiao, Y. Catalytic dehydrogenation cracking of crude oil to light olefins by structure and basicity/acidity adjustment of bifunctional metal/acid catalysts. *Fuel.* **2023**, *334*, No. 126808.
(43) Premkumar, P.; Saravanan, C. G.; Nalluri, P.; Seeman, M.; Vikneswaran, M.; Madheswaran, D. K.; Josephin, J. S. F.; Chinnathambi, A.; Pugazhendhi, A.; Varuvel, E. G. Production of liquid hydrocarbon fuels through catalytic cracking of high and low-density polyethylene medical wastes using fly ash as a catalyst. *Process Saf. Environ. Prot.* **2024**, *187*, 459−470.
(44) Lovás, P.; Hudec, P.; Jambor, B.; Hájeková, E.; Horňáček, M. Catalytic cracking of heavy fractions from the pyrolysis of waste HDPE and PP. *Fuel.* **2017**, *203*, 244−252.
(45) Turkyilmaz, A.; Isinkaralar, K.; Dogan, M.; Kizilduman, B. K.; Biçil, Z. Production, characterization, and hydrogen storage properties of activated carbon from horse chestnut shell. *Sustainable Chem. Pharm.* **2024**, *40*, No. 101634.
(46) Jiang, M.; Su, Y.; Yang, L.; Qi, P.; Wang, J.; Xiong, Y. Study on H_3PO_4-activated carbon catalytic co-pyrolysis of bamboo and LDPE to poly-generation syngas and aromatics at low temperature. *Fuel* **2024**, *369*, No. 131737.
(47) Khosravi, K.; Alavi, S. M.; Rezaei, M.; Akbari, E.; Varbar, M.; Pirshahid, M. B. Influence of nickel contents on synthesis gas production over nickel-based catalysts supported by treated activated carbon in dry reforming of methane. *Int. J. Hydrogen Energy* **2024**, *69*, 358−371.

https://doi.org/10.1021/acsomega.4c08111
ACS Omega 2025, 10, 14699−14722

(48) Yao, N.; Zhang, C.; Luo, C.; Wang, J.; Zeng, Z.; Li, L. Optimization and analysis of biomass carbon loaded metal catalyst for catalytic cracking of toluene. *Diam. Relat. Mater.* **2023**, *136*, No. 109987.

https://doi.org/10.1021/acsomega.4c08111
ACS Omega 2025, 10, 14699−14722